"ANALYSIS OF SHOCKWAVE BOUNDARY LAYER INTERACTION AND ASSESSMENT OF PASSIVE FLOW CONTROL DEVICE"

(Sub Code: 10AE85)

A Project Report Submitted To

VISVESVARAYA TECHNOLOGICAL UNIVERSITY
BELAGAVI

in partial fulfillment of the requirement for the award of the degree

BACHELOR OF ENGINEERING
in
AERONAUTICAL ENGINEERING

2017-18

Submitted By

ABHISHEK DHIMAN	**(1DS14AE003)**
CHETHAN S	**(1DS14AE017)**
DEVANURU SAIRAM BHARADWAJ	**(1DS14AE021)**
D SHOBITHA	**(1DS14AE063)**

Under the guidance of

Mr. C MANISANKAR
Sr. SCIENTIST
Expt. Aerodynamic division
CSIR-NAL, Bengaluru-560017

Dr. A AROKKIASWAMY, Professor,
HoD, Department of Aeronautical Engg.
Dayananda Sagar College of Engineering,
Bengaluru-560078

DAYANANDA SAGAR COLLEGE OF ENGINEERING
DEPARTMENT OF AERONAUTICAL ENGINEERING
Kumaraswamy Layout, Bengaluru-560078

CERTIFICATE

Certified that the project work entitled **"ANALAYSIS OF SHOCKWAVE BOUNDARY LAYER INTERACTION AND ASSESSEMENT OF PASSIVE FLOW CONTROL DEVICE"** carried out by Mr. **ABHISHEK DHIMAN (1DS14AE003),** Mr. **CHETHAN S (1DS14AE017),** Mr. **DEVANUR SAIRAM BHARADWAJ (1DS14AE021),** Ms. **D SHOBITHA (1DS14AE063),** in partial fulfillment for the award of **Bachelor of Engineering** in **Aeronautical Engineering** of Visvesvaraya Technological University, Belagavi, during the year 2017-18. It is certified that all corrections/suggestions indicated for internal assessment have been incorporated in the report deposited in the departmental library. The project report has been approved as it satisfies the academic requirements in respect of project work prescribed for the said degree.

Signature of the Guide	Signature of the HOD	Signature of the Principal
(Dr. A Arokkiaswamy)	**(Dr. A Arokkiaswamy)**	(**Dr. C P S Prakash**)

Name of the examiners	Signature
1)	
2)	

DECLARATION

We, Mr. ABHISHEK DHIMAN (1DS14AE003), Mr. CHETHAN S (1DS14AE017), Mr. **DEVANUR SAIRAM BHARADWAJ (1DS14AE021),** Ms. **D SHOBITHA (1DS14AE063),** hereby declare that, this dissertation work entitled **"ANALYSIS OF SHOCKWAVE BOUNDARY LAYER INTRACTION AND ASSESSMENT OF PASSIVE FLOW CONTROL DEVICE"** has been carried out by us under the guidance of **Dr. A Arokkiaswamy,** Professor, HoD, Department Of Aeronautical Engineering, in partial fulfillment of the requirement of the degree **Bachelor of Engineering in Aeronautical Engineering**, of Visveswaraya Technological University, Belagavi.

Place: BENGALURU
Date:

ABHISHEK DHIMAN
(1DS14AE003)

CHETHAN S
(1DS14AE017)

DEVANUR SAI RAM BHARADWAJ
(1DS14AE021)

D SHOBITHA
(1DS14AE063)

ACKNOWLEDGEMENT

Before introducing our thesis work, we would like to thank the people without whom the success of this thesis would have been only a dream.

It is with great pleasure, we extend our gratitude and thanks to **Dr. C P S Prakash**, Principal, Dayananda Sagar College of Engineering, for his encouragement throughout the project.

We express our deep sense of gratitude and indebtedness to **Dr. A Arokkiaswamy**, Professor and HOD, Department of Aeronautical Engineering, for his valuable guidance, continuous assistance and in the critical appraisal of the thesis and also for providing the facilities required for the completion of this project work.

We are very thankful to **Dr. S B Verma**, Deputy Head, Experimental Aerodynamics Division, CSIR-NAL for his technical support for the present project.

We are very grateful to **Mr. C Manisankar**, Scientist, Experimental Aerodynamic Division, CSIR-NAL for being a great source of knowledge and help during design and analysis stage and guidance in spite of his busy schedule.

Our sincere thanks to **Dr. T K Pradeepa**, project coordinator for his encouragement and guidance.

We express our heartfelt thanks to all our family members and friends and all those who have directly or indirectly helped us during our course.

ABHISHEK DHIMAN (1DS14AE003)
CHETHAN S (1DS14AE017)
SAIRAM BHARADWAJ (1DS14AE021)
D SHOBITHA (1DS14AE063)

ABSTRACT

Shock wave boundary layer interaction is an unavoidable/undesirable event occurring in high speed flows/high speed air breathing propulsion systems. This simulates boundary layer simulations due to adverse pressure gradients which therefore leads effects like such as wall pressure loading, high local wall heating, increased drag coefficient, reduced mass flow ingestion, lower-pressure recovery and inlet unstart conditions.

The proposed study aims to perform numerical flow simulation of shockwave boundary layer interactions on a flat plate and validate the results with the available experimental data. 3D Grid Independent Study is performed for a typical case of freestream Mach number 2.05. This study involves a passive flow control mechanism which includes a Rectangular Vane Type Micro Vortex Generator that has shown good potential to reduce the shock induced flow separation. The device height spanned 37.78% of the local boundary layer thickness of no-control case. Array of rectangular vane type micro vortex generators is placed at 5.5δ upstream of the separation location of no-control case. The size of recirculation zone in the shockwave boundary layer interaction flows depends on various parameters. The influence of Mach number variation on recirculation zone thickness is studied and is observed that increase in Mach number results in the increase in recirculation zone thickness.

TABLE OF CONTENTS

LIST OF TABLES

LIST OF FIGURES

TABLE OF ABBREVIATIONS

ANSYS	Analysis System
BLT	Boundary Layer Thickness
CFD	Computational Fluid Dynamics
FDM	Finite Difference Method
FEM	Finite Element Method
FVM	Finite Volume Method
FSS	Free Shock Separation
LE	Leading Edge
MVG	Micro Vortex Generator
PDE	Partial Differential Equation
RVG	Rectangular Vortex Generator
RSS	Restricted Shock Separation
RANS	Reynolds Averaged Naiver Strokes
SST	Shear Stress Transport
SWBLI	Shock Wave Boundary Layer Interaction
SA	Spalart- Allmaras
3D	Three Dimensional
TE	Trailing Edge
TBL	Turbulent Boundary Layer
2D	Two Dimensional
VG	Vortex Generator
WA	Wary- Agarwal

TABLE OF NOMENCLATURE

SI No.	PARAMETERS	SYMBOLS	UNITS
1	Specific Heat Ratio	γ	-
2	Universal Gas Constant	R	J/kg K
3	Reynolds No.	Re	-
4	Stagnation Pressure	P_0	Pa
5	Inlet Static Pressure	P_1	Pa
6	Stagnation Temperature	T_o	K
7	Inlet Static Temperature	T_1	K
8	Inlet Mach No.	M_1	-
9	After shock Mach No.	M_2	-
10	Speed of Sound	a	m/s
11	Free stream velocity	U_∞	m/s
12	Inlet velocity	V_1	m/s
13	After shock velocity	V_2	m/s
14	Analytical oblique shock angle	β	degrees
15	Experimental oblique shock angle	β_{actual}	degrees
16	Density	ρ	Kg/m^3
17	Wedge generator angle	Θ	degrees
18	Turbulence Kinetic energy	k	$m^2/\ s^2$
19	Rate of dissipation of Turbulence (K.E)	ε	$m^2/\ s^3$
20	Specific rate of dissipation of Turbulence (K.E)	ω	s^{-1}
21	Turbulence / Eddy viscosity	ν_τ	$m^2/\ s^1$
22	Boundary layer thickness	δ	mm
23	Boundary layer thickness at separation	δ_s	mm
24	Impingement point w.r.t plate L.E.	X_{imp}	mm
25	Separation point w.r.t plate L.E.	X_s	mm
26	Interaction length	X_{IL}	mm
27	Recirculation zone height	H_B	mm
28	Vortex generator height	h	mm
29	Mach stem length	H_m	mm

CHAPTER-1

INTRODUCTION

The interactions of a shock-wave with a boundary-layer can have a significant influence on high speed vehicles. Drag rise, flow separation, adverse aerodynamic loading, high aerodynamic heating, and poor engine inlet performance are but a few examples of its deleterious influence.

The purpose of this study is to investigate the use of a novel type of flow control called Micro-Rectangular Vane Type Vortex Generator which is able to offer benefits in suppressing the SWBLIs as well as improving the boundary layer health. This mechanism is robust, independent of power source and also cost effective.

1.1. OBJECTIVES

The main objectives of the present project work are following:

- To carry out a validation case of shock wave boundary layer interaction over a flat plate.
- To conduct viscous 2-D and 3-D numerical flow simulation (CFD analysis) of a SWBLI over a flat plate.
- To perform grid independent study for a typical case of free stream Mach number of 2.05.
- To investigate the flow characteristics of a rectangular vane type micro vortex generators.
- To study the capabilities of the rectangular vane type micro vortex generators for controlling the flow separation induced by SWBLI.
- To study the effect of variation of freestream Mach number on the recirculation zone thickness.

1.2. SCOPE OF THE WORK

- Analytical calculations were made to determine the velocity, temperature, pressure values at inlet.

- The 2D and 3D geometries were generated using ANSYS 15.0. A structured mesh has been generated using Hexa-Dominant method to capture the flow field.
- A numerical analysis has been carried out in CFD – Fluent. At inlet of the fluid domain, initial static pressure, static temperature and velocity are given as boundary conditions.
- CFD is used to solve the defined problem, the K-ω SST model is opted for turbulence model.

1.3. PROBLEM DEFINITION

The definition of the current problem is to address the issues related to the SWBLI and effects of Micro-Vortex Generators on the Shock Induced Flow Separation. So, the design and analysis of SWBLI on a flat plate is carried out with and without employing Rectangular Vane type Micro Vortex Generators.

1.4. ORGANIZATION OF THESIS

Following the introduction chapter, this thesis will give a detailed procedure of the CFD analysis to study the phenomena of Shockwave Boundary Layer Interaction over a flat plate and to assess the capability of a Micro-Rectangular Vane Type Vortex Generators in reducing the shock induced separation.

Chapter 2 presents the background understanding on SWBLI and various flow control techniques.

Chapter 3 provides an extensive review on the previous studies involving SWBLI phenomena and several micro vortex generators.

Chapter 4 talks about the design methodology, inputs and requirements, calculations, 2D and 3D Geometry.

Chapter 5 gives a detailed description about CFD. It explains CFD governing equations, procedure, explicit and implicit methods, types of turbulence models, discretization types, meshing details, boundary conditions, analysis and solution. Grid independent study is also highlighted in this section.

Chapter 6 CFD results are studied and discussed.

Chapter 7 draws conclusion also including the recommendation of future work.

CHAPTER-2

SHOCKWAVE BOUNDARY LAYER INTERACTION

2.1. INTRODUCTION

The prominent problem faced by high speed flow intakes or on lifting surfaces is the complex phenomenon of shock wave boundary layer interactions (SWBLI) which leads to boundary layer separation and adverse pressure gradients. The goal is to minimize the total pressure losses. Therefore, a fundamental understanding of this physical phenomenon is important for the development of improved techniques to control their counterproductive effects.

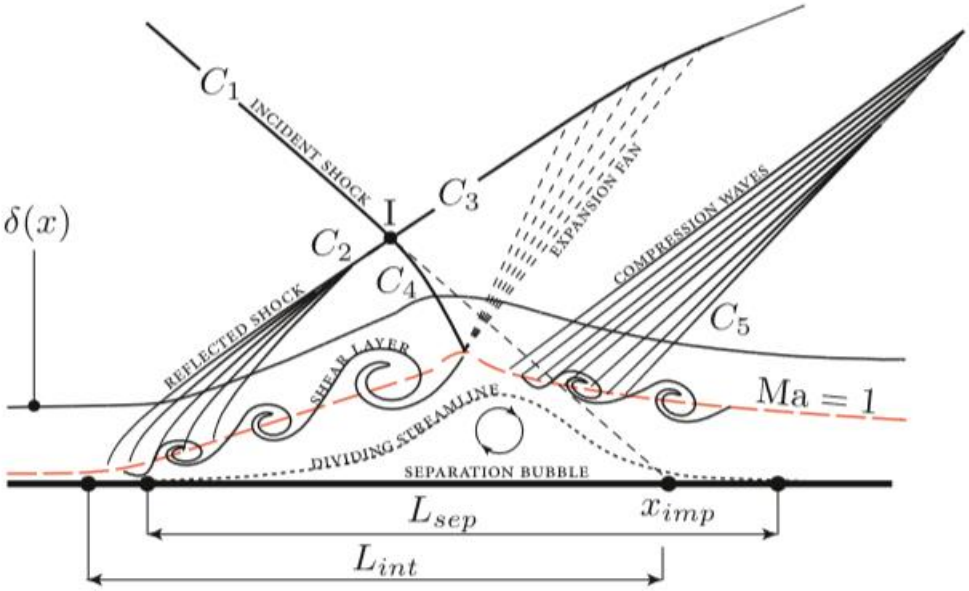

Fig 2. 1 Phenomena of Shockwave Boundary Layer Interaction[1]

Fig.2.1 shows the schematic of the incident shock induced separation when undergoing regular reflection. The impingement of the incident shock wave(C1) causes a large pressure difference across it hence induces the boundary layer to separate due to the consequent effect of severe adverse pressure gradient. The separation occurs well ahead the impingement location, Ximp. The upstream propagation of the pressure gradient within the subsonic part of the turbulent boundary-layer (TBL) induces compression waves in the supersonic part of the TBL, which coalesce to the reflected shock (C2). This reflected shock (C2) intersects the incident shock (C1) at 'I' and it forms transmitted shocks (C3 and C4).

The shock (C4) penetrates into the separated shear layer and is reflected as an expansion fan which causes the flow to reattach. This flow turning – reattachment process results in the formation of compression waves that merge together to form a reattachment shock (C5). Finally, the boundary layer reaches equilibrium downstream of the SWBLI[1][2].

If the strength of the induced shock (C1) reaches the detachment limit for a given freestream Mach number, the intersection point 'I' gets replaced with a normal shock which is known as a Mach Stem. In both the causes the separation formed acts as an obstacle to the incoming flow.

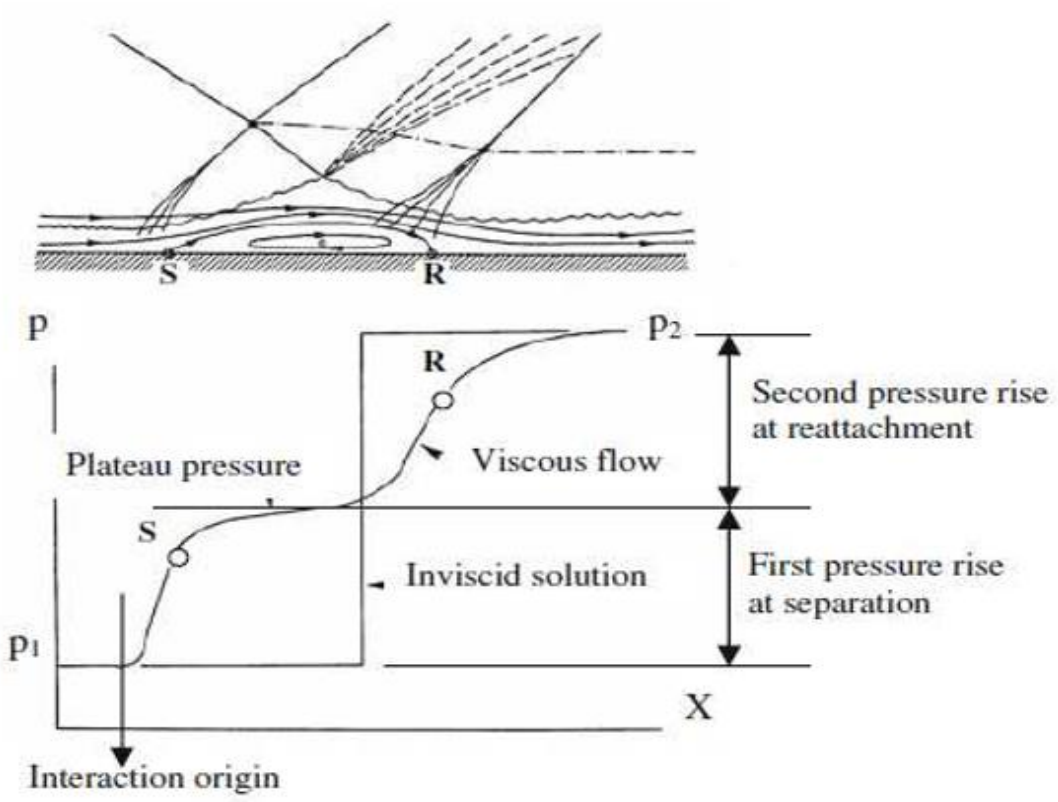

Fig 2. 2 Static Pressure along Plate Length showing First and Second Pressure rise[3]**.**

Fig.2.2. shows the separation point is denoted by S and further downstream exists a recirculating 'bubble'. This area is bounded by a layer called dividing streamline (S) that separates the recirculating region from the incoming flow. The dividing streamline originates from point S and ends at the reattachment point R. Strong mixing takes place in the detached shear layer emanating from S and causes mechanical energy transfer to occur from outer high-speed flows into the separated region. As a result, the velocity on the dividing streamline (S) increases gradually until it approaches the reattachment point (R) where deceleration starts[3].

2.2. EFFECTS OF SWBLI

2.2.1. CONTROL SURFACES

In high speed vehicles, high flap angles are needed to produce the required control forces on the incoming flow. As a result of the high flap angles, flow separation will occur upstream of the control surface due to the high adverse pressure gradients followed by generation of complex shock-wave structures. The separation region reduces the effective area of the flap, consequently minimizing the maneuverability of the vehicle.

The generated shock-waves that impinge on the vehicle's body will also increase the local heating rates. Another problem is the flow separation and unsteadiness also contribute to the rise in aerodynamic drag. When all of these effects combine with the fluctuating pressure loads, the result is severe enough to cause premature structural fatigue for high speed vehicles.

2.2.2. HYPERSONIC VEHICLES

Hypersonic flows are synonymous with high-Mach number flows and therefore are characterized by very strong shock waves. Hypersonic vehicles tend to fly at high altitudes so that convective heating levels can be managed. Thus, the characteristic Reynolds numbers tend to be low and boundary layers are usually thick. In addition, shear heating in hypersonic boundary layers increases the temperature and viscosity, which also increases the thickness. The low Reynolds number and the relative stability of hypersonic boundary layers mean that many practical hypersonic flows are laminar or transitional. If the flow is turbulent, it is often only marginally turbulent. Therefore, hypersonic flows are particularly susceptible to shock wave–boundary-layer interactions.

The design of a hypersonic vehicle – whether a planetary-entry capsule, a high lift reentry vehicle such as the Space Shuttle, or a scramjet-powered aircraft – is dominated by aerodynamic heating. Blunt bodies such as planetary-entry capsules are protected from large heat fluxes by the thick boundary layer that insulates the vehicle from the high-temperature stagnation-region flow. Anything that interrupts this insulating layer (e.g., an impinging shock wave) can be catastrophic to a vehicle.

SBLIs can cause flow separation and change the effectiveness of control surfaces on hypersonic vehicles. The flow inside the isolator of a scramjet engine is dominated by interactions between shock waves and turbulent-boundary layers, and these interactions are responsible for raising the pressure and preventing engine unstart due to fluctuations in

engine-operating characteristics. Thus, SBLIs can either destroy a hypersonic vehicle or be responsible for its effective operation. The development of future hypersonic vehicles depends on high-fidelity simulation tools for their design and optimization. Current computational fluid dynamics (CFD) methods can predict many aspects of practical hypersonic flows. However, the accurate simulation of SWBLI flows remains a severe challenge for the best available CFD methods[4].

2.2.3. ROCKET NOZZLES

Rocket engine the nozzle is highly over expanded and an internal flow separation takes place, characterized by a shock wave boundary layer interaction(SWBLI), which causes the shedding of vorticial structures and unsteadiness in the shock wave position. In the nozzle design community, flow separation is considered dangerous, since it produces dynamic side-loads that reduce the safe life of the engine and can lead to a failure of the nozzle structure. The need to improve nozzle performance under over expanded conditions and to mitigate the side loads fostered several experimental studies. All these studies revealed two distinct separation processes: the free shock separation (FSS), in which the boundary layer separates from the nozzle wall and never reattaches, and the restricted shock separation (RSS), characterized by a closed recirculation bubble and the reattachment of the shear layer to the wall[5].

2.2.4. ENGINE INLETS

The prominent issue facing hypersonic flights is the engine limitations due to the occurrence of the shock-wave/boundary layer interactions (SBLIs) in the supersonic portion of the flow inside the supersonic engine inlets. The interactions are caused by a number of oblique and normal shock waves interacting with the boundary layer of the inlet flow consequently causing boundary layer separation and unsteady flow due to severe adverse pressure gradients.

When the shock train reflects off the inlet walls, it interacts with the developing boundary layer and causes SWBLI effects. The interactions induce adverse pressure gradients that results in boundary layer separation at several locations downstream the inlet.

The thickening of the boundary layer due to the separation decreases the effective throat area and could lead to inlet unstart. Another contributing factor to the inlet unstart is the flow distortion and unsteadiness which translates to large oscillating structural loads that could also result in structural fatigue. Hence the SWBLIs effects in mixed compression inlet

affect not only the propulsion system but also endanger the structural strength of any aero-vehicle[3].

2.3. FLOW CONTROL TECHNIQUES

The aim of the control mechanisms is to prevent the shock induced separation and to stabilize the oscillating shock. The momentum of the turbulent boundary layer appears to be an important factor affecting the upstream influence of the shock as well as the resistance of the boundary layer towards separation. In these passive flow control mechanisms, adding momentum to the boundary layer prior to the interaction with shock, is beneficial[3].

2.3.1. BLEED SYSTEMS

Bleed system is widely used. Bleeding the flow at the shock impingement point can actually reduce separation by thinning out the boundary layer. So, to perform this certain mass flow must be removed/taken out to actually make this technique work. To compensate for this loss in mass flow, the inlet area has to be increased weight and drag. And to passive control devices are developed which are simple, cost effective and robust (larger nacelle contributes to additional weight).

2.3.2. SUCTION

Suction is applied locally inside the interaction region or in the immediate vicinity. It is done through drilling holes perpendicularly to the surface. The other way of implementing this method is at a certain distance upstream (usually specified in scale of the boundary layer thickness, δ) of the shock impingement. This will produce a fuller velocity profile and more robust boundary layer towards separation.

2.3.3. FLUID INJECTION

This is done by applying fluid injection through a porous plate or several slots positioned upstream of the shock impingement location.

2.3.4. VORTEX GENERATORS

A vortex generator (VG) is an aerodynamic device, consisting of a small vane usually attached to a lifting surface or a rotor blade of a wind turbine. VGs may also be attached to some part of an aerodynamic vehicle such as an aircraft fuselage. When the airfoil or the

body is in motion relative to the air, the VG creates a vortex, which, by removing some part of the slow-moving boundary layer in contact with the airfoil surface, delays local flow separation and aerodynamic stalling, thereby improving the effectiveness of wings and control surfaces, such as flaps, elevators, ailerons, and rudders.

Vortex generators are most often used to delay flow separation. Conventional VGs which have the height of the boundary layer thickness, δ have been used for decades to control the separation by increasing the near-wall momentum by transferring the high momentum flow from the outer region into the lower momentum region, at the wall. This type of flow control, which is usually characterized as passive flow control, so doesn't require the addition of extra energy to the system nor it needs any actuators. These are becoming more favorable despite active devices have their own attractions. More researches proved that the micro VGs, termed after having the height less than the boundary layer thickness, are able to outperform the performance of the conventional.

Benefits of Vortex Generators:

- Lower lift off speed
- Lower stall speeds
- Improved controllability
- Easy installation
- Improved safety

CHAPTER-3

LITERATURE REVIEW

During the literature review on design of various Micro-Vortex Generators and its effects on Shockwave Boundary Layer Interactions in various high-speed flows, it is observed that various studies and analysis

S. B. Verma and **C. Manisankar**[6] investigated the performance of several Micro-Vortex Generators of height 30% and a ramp-vane of height 50% of the local boundary layer thickness(δ) of no-control case which was implemented at 10δ upstream of separation location.

Shashi.B. Verma and **Manisankar**[2] conducted experiments by splitting the trapezoidal control configuration into rectangular vane type control devices and found that a local pressure relieving effect is created and also found out that the height of the Vortex Generators is significant to control the extent of separation.

S. B. Verma and **A. Hadjadj**[7] focused on the flow control mechanisms by implementing various VG configurations which effect the flow unsteadiness, bow-shock strengths and reduce the overall sound pressure levels by 4.5dB.

Amjad Ali Pasha[8] studied the effect of deflection angle, the Reynolds Number, the wall temperature and the Mach Number on the recirculation zone in hypersonic SWTBLI flows using CFD as a tool for compression ramp in which it was observed that by keeping the above-mentioned parameters constant, a decrease in freestream Mach number results in larger length of the recirculation zone.

Mohd R. Saad, Hossein Zare-Behtash, Azam Che-Idris and **Konstantinos Kontis**[9] stated that the height of the Micro-Vortex Generators should be in the range 30% - 90% of the local boundary layer thickness, which are embedded inside the boundary layer, which is intended to reduce parasitic drag relative to the conventional full-size VG.

Francis K. Acquaye[10] evaluated various turbulence models for three different supersonic flow conditions and compared WA, SA, and SST k-ω models and found out that SST k-ω model made accurate predictions of the flow separation in SWBLI.

Mohd R. Saad[3] investigated the micro ramps in detail using various flow diagnostic methods. The oil-flow and oil-dot visualization enabled technique the visualization of the

detail structures. A significant alteration in the separation region and minimization in the reversed flow region was also observed.

Frank K. Lu, Qin Li, Yusi Shih, Adam J. Pierce and Chaoqun Liu[11] performed an assessment of various micro vortex generator configurations and studied that these MVG adds momentum to the boundary layer which acts as a beneficiary factor in reducing the shock induced separation.

Thomas Herges, Erik Kroeker, Greg Elliott and **Craig Dutton**[12] investigated micro ramp array at Mach 1.4 and its effects of on normal SWBLI. The height of the vortex generators was scaled to 40% of the incoming boundary layer thickness. The incompressible displacement thickness was decreased for the SBLI with the micro-ramp array relative to the no-array case.

The survey of literature indicates that specific and focused research work has been carried out all over the world on the flow physics in the complex phenomena SWBLI. It includes study of various parameters affecting the boundary layer thickness, separation location and recirculation zone height. Most efforts to determine the optimum height of the micro vortex generators.

CHAPTER-4

METHODOLOGY

4.1. DESIGN SPECIFICATIONS

The flat plate model used is of 340mm length with 110mm width. An incident shock wave generated using a fixed wedge of 220mm width and of 51.683mm length with a flow turning angle of 14˚, is made to impinge on the flat plate.

Table 4.1. Design Input Requirements

Specific Heat Ratio, γ	1.4
Universal Gas Constant, R	287 J/kg K
Stagnation Pressure, P_0	208.5 kPa
Stagnation Temperature, T_o	298 K
Reynolds Number based on plate length, *Re/L*	25.257*10^6
Inlet Mach Number, M_1	2.05
P_1/P_0	0.1182
T_1/T_o	0.5433
ρ/ρ_0	0.21762
Inlet Static Pressure, P_1	246.5 kPa
Inlet Static Temperature, T_1	161.91 K
Speed of Sound, a	255.061 m/s
Inlet Velocity, U_∞	523 m/s
P_2/P_1	2.1079
T_2/T_1	1.2522
M_2	1.5325

4.2. METHODOLOGY FOR DESIGN AND ANALYSIS

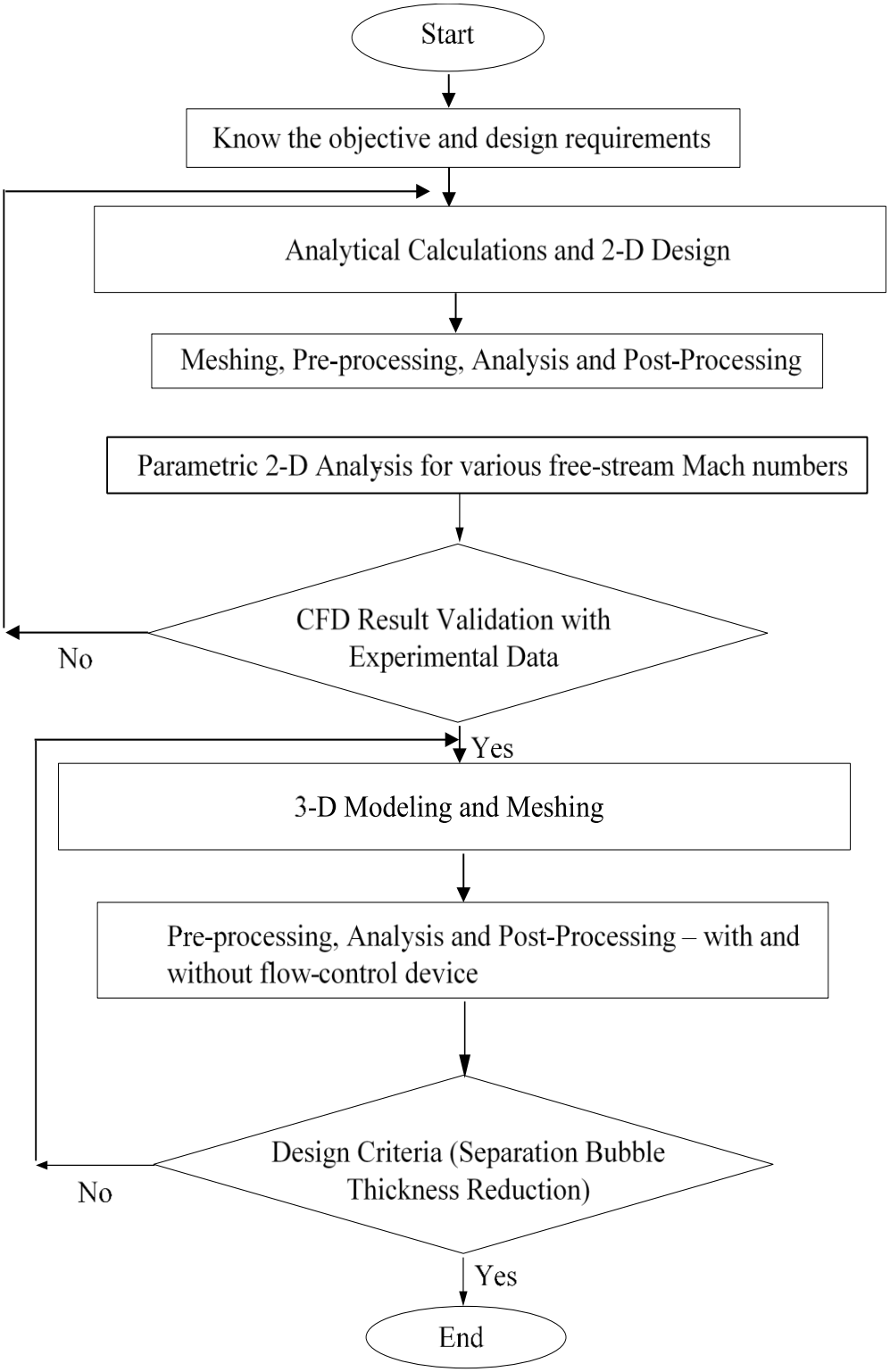

4.3. THEORETICAL CALCULATIONS

This design process is based on the fundamental principles of fluid flow with continuity, momentum and energy equations. The turbulent boundary layer over a flat plate is made to interact with the incident oblique shock wave generated from a wedge with a flow turning angle of 14°, which leads to formation of recirculation zone. The strength of shock wave is strong enough to induce flow separation.

During this process pressure, temperature, density, flow velocity and shock angle are calculated for a particular free-stream Mach number. Design procedure and calculation for the above referred input parameters are presented in the calculation.

4.3.1. FORMULAS USED

ISENTROPIC RELATIONS:

$$\frac{Po}{P_1} = [1 + (\gamma - 1)/2 * M^2]^{\frac{\gamma}{(\gamma-1)}} \quad (4.1)$$

$$\frac{To}{T_1} = [1 + (\gamma - 1)/2 * M^2] \quad (4.2)$$

M = Mach Number

Po = Total Pressure

To = Total Temperature

T_1 = Static Temperature

γ = Specific Heat Ratio

OBLIQUE SHOCKWAVE RELATIONS:

$$\frac{\rho_2}{\rho_1} = \frac{(\gamma+1)*{M_1}^2*(sin^2\beta)}{2+(\gamma-1)*{M_1}^2*(sin^2\beta)} \quad (4.3)$$

$$\frac{P_2}{P_1} = \frac{2*\gamma*{M_1}^2*(sin^2\beta)-(\gamma-1)}{(\gamma+1)} \quad (4.4)$$

$$\frac{T_2}{T_1} = \frac{P_2}{P_1} * \frac{\rho_1}{\rho_2} \quad (4.5)$$

$$M_2{}^2 * sin^2(\beta - \theta) = \frac{(\gamma-1)*M_1{}^2*sin^2(\beta)+2}{2*\gamma*M_1{}^2*sin^2(\beta)-(\gamma-1)} \quad (4.6)$$

$$tan\theta = 2 * cot\beta * \frac{M_1{}^2*sin^2(\beta)-1}{M_1{}^2*(\gamma+\cos 2\beta+2)} \quad (4.7)$$

θ=shock generator angle

β=oblique shock angle

M_1=upstream mach.no

M_2=downstream mach.no

P_1=upstream pressure

P_2= downstream pressure

4.4. 2-D DESIGN

Fig 4.1. shows the 2-D design with the named selections. The domain size is kept 285x340 mm. The wedge leading edge is at 150mm from the inlet and 200 mm from the far field.

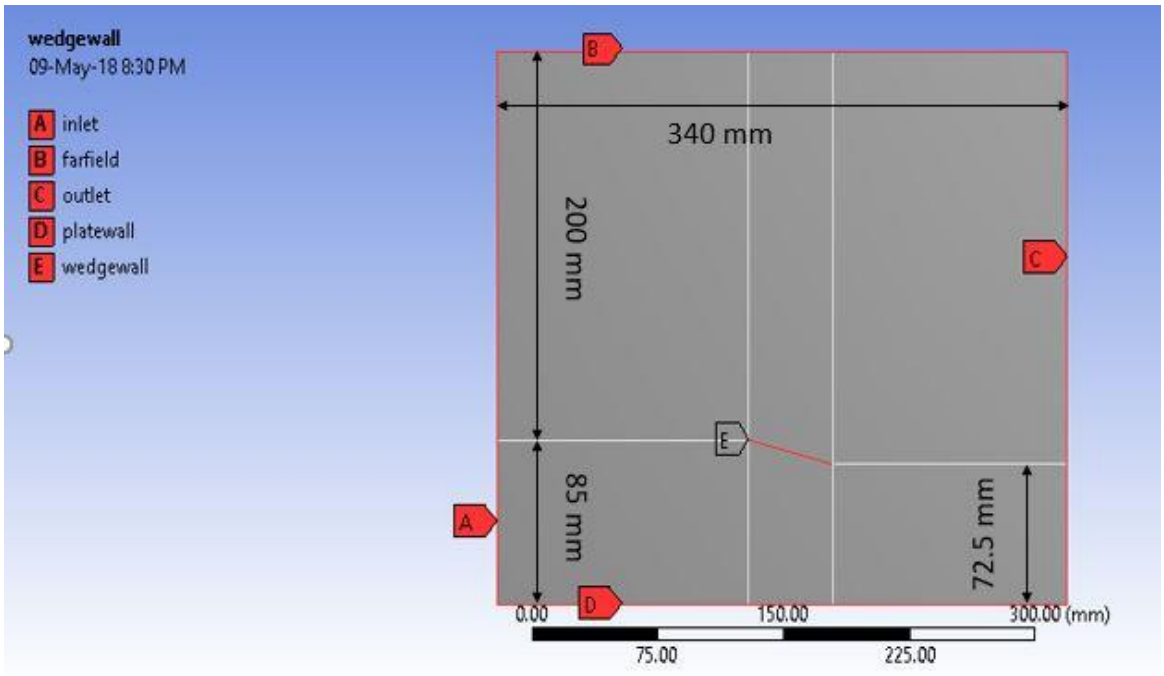

Fig. 4.1 2-D Plate Geometry

4.5. 3D MODELING

3-D modeling is done using ANSYS 15.0. A flat plate of length 340mm is made and extruded 110 mm. A fluid domain of volume 840x360x500 mm is created. Wedge of 154x160x12.5 with a turning angle of 14˚ is made. Fig. 4.2. shows the 3-D geometry divided into several blocks.

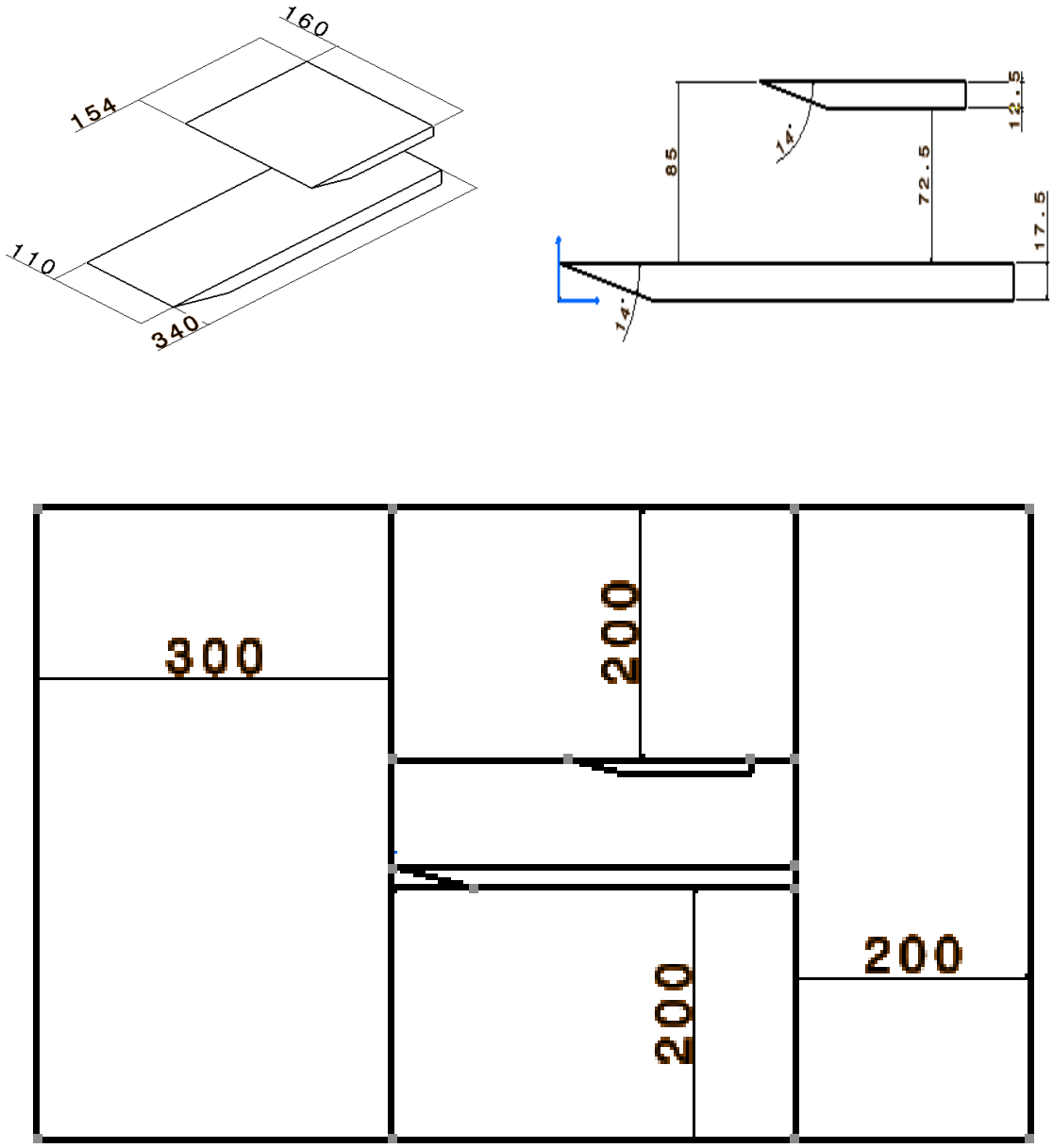

Fig. 4.2. Schematic of Flat Plate and Wedge

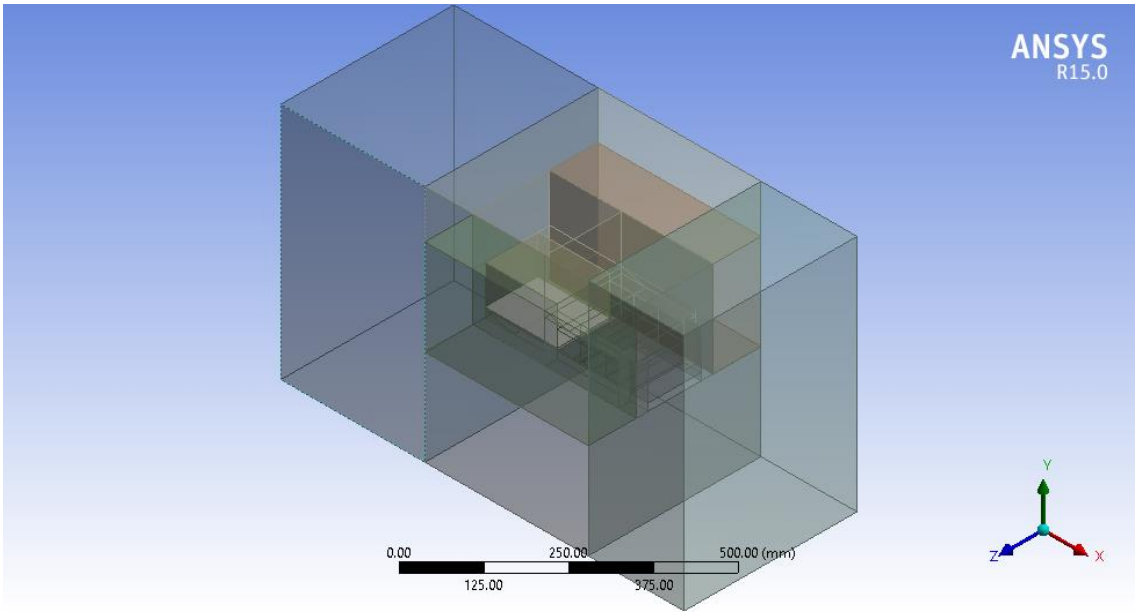

Fig. 4.3. 3-D Geometry Isometric View

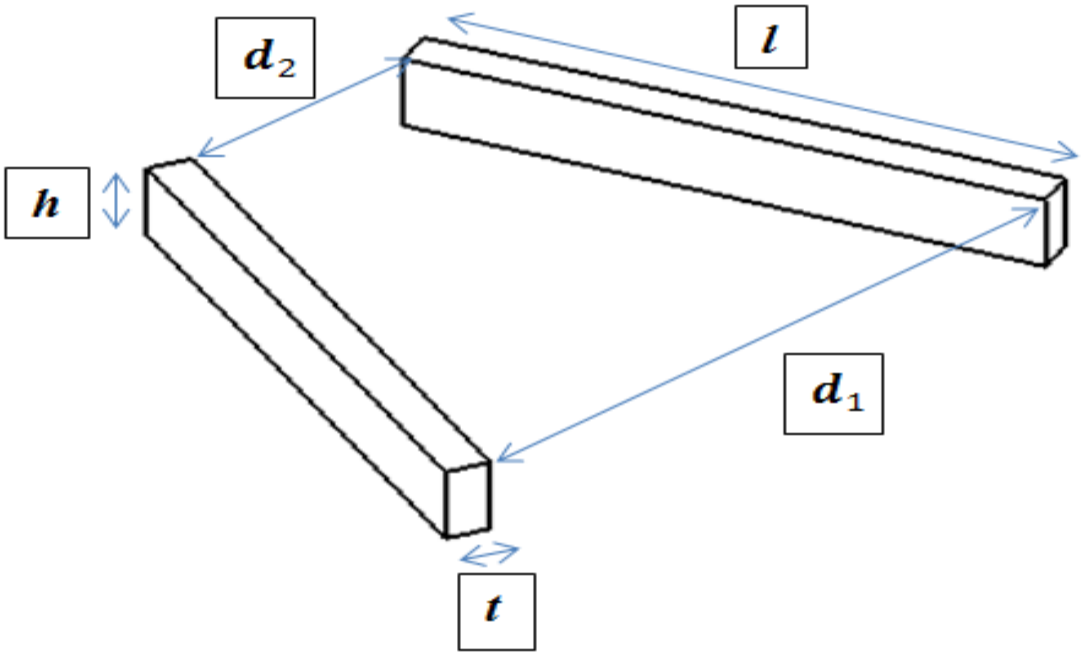

Fig.4.4. Schematic of RVG

Table 4.2 Vortex Generators Parameters

PARAMETER	RVG, h/δ=0.23	RVG, h/δ=0.4
Height (h) mm	1	1.7
Length (l) mm	7.13	7.13
d_1	3	3
d_2	7.9	7.9
Thickness (t) mm	0.5	0.5

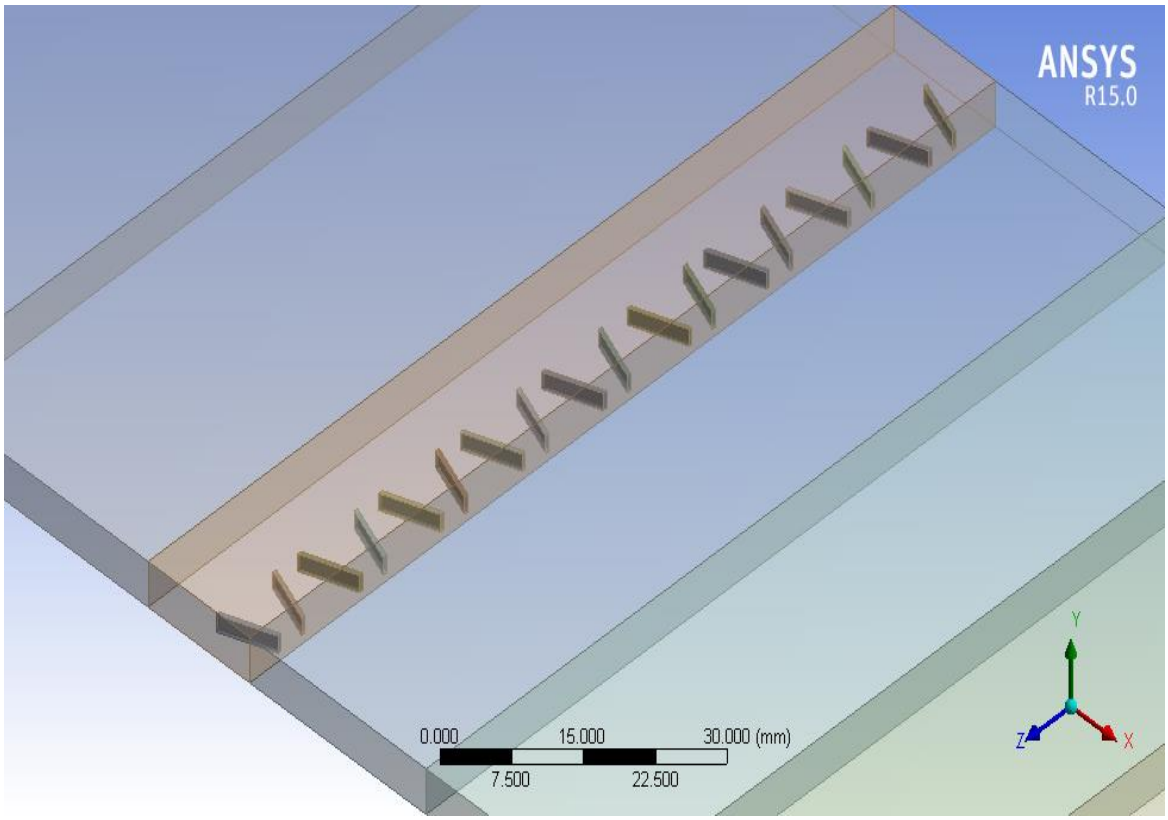

Fig. 4.5. Array of RVG on Plate Surface

Fig.4.4. shows the arrangement of RVG on the surface of the Flat Plate at a distance of 5.5δ upstream of the Separation line. The RVGs produce counterrotating vortices that add momentum to TBL.

CHAPTER-5

COMPUTATIONAL FLUID DYNAMICS

Computational fluid dynamics (CFD) is the science of predicting fluid flow, heat transfer, mass transfer, chemical reactions, and related phenomena by solving the mathematical equations which govern these processes using a numerical process. Computers are used to perform the calculations required to simulate the interaction of liquids and gases with surfaces defined by boundary conditions. With high-speed super computers, better solutions can be achieved. Ongoing research yields software that improves the accuracy and speed of complex simulation scenarios such as transonic or turbulent flows. Initial experimental validation of such software is performed using a wind tunnel with the final validation coming in full-scale testing, e.g. flight tests. The result of CFD analyses is relevant engineering data used in, Conceptual studies of new designs, Detailed product development, Troubleshooting, Redesign.

Fluid dynamics is the science of fluid motion. The study of the fluid flow can be possible in three various ways as 1) Experimental 2) Theoretical and 3) Numerically. The numerical approach is called Computational fluid dynamics. CFD uses numerical methods and algorithms to solve and algorithms to solve and analyze problems that involve fluid flows by using computers.

5.1. CFD ANALYSIS PROCESS

The general process for performing a CFD analysis is outlined below so as to provide a reference for understanding the various aspects of a CFD simulation. The process includes:

- Formulate the Flow Problem
- Model the Geometry and Flow Domain
- Establish the Boundary and Initial Conditions
- Generate the Grid
- Establish the Simulation Strategy
- Establish the Input Parameters and Files
- Perform the Simulation
- Monitor the Simulation for Completion

- Post-process the Simulation to get the Results
- Make Comparisons of the Results
- Repeat the Process to Examine Sensitivities
- Document

5.2. WORKING OF CFD

CFD codes are structured around the numerical algorithms that can be tackled for fluid problems. In order to provide easy access to their solving power all commercial CFD packages include sophisticated user interfaces input problem parameters and to examine the results. Hence all codes contain three main elements:

5.2.1. PRE-PROCESSOR

Pre-processor consists of the input of the flow problem to a CFD program by means of an operator friendly interface and the subsequent transformation of this input into a form suitable for use by the solver. The region of fluid to be analyzed is called the computational domain and it is made up of a number of discrete elements called the mesh (or grid). After the mesh generation, to define the properties of fluid and to specify appropriate boundary condition.

5.2.2. SOLVER

Solver calculates the solution of the CFD problem by solving the governing equations. The equations governing the fluid motion are Partial Differential Equations (PDE), made up of combinations of the flow variables (e.g. velocity and pressure) and the derivatives of these variables. Computers cannot directly produce a solution of it. Hence the PDEs must be transformed into algebraic equations. This process is known as numerical discretization. There are four methods for it as 1) Finite difference method 2) Finite element method and 3) Finite volume method and 4) Spectral method. The finite difference method and the finite volume method both produce solutions to the numerical equations at a given point based on the values of neighboring points, whereas the finite element method produces equations for each element independently of all other elements.

5.2.3. POST-PROCESSOR

It is used to visualize and quantitatively process the results from the solver part. In a CFD package, the analyzed flow phenomena can be presented in vector plots or contour plots to display the trends of velocity, pressure, kinetic energy and other properties of the flow.

5.3. DISCRETIZATION METHODS IN CFD

There are three Discretization methods in CFD:

- Finite difference method (FDM)
- Finite volume method (FVM)
- Finite element method (FEM)
- Spectral method

5.3.1. FINITE DIFFERENCE METHOD (FDM)

A finite difference method (FDM) discretization is based upon the differential form of the PDE to be solved. Each derivative is replaced with an approximate difference formula (that can generally be derived from a Taylor series expansion). The computational domain is usually divided into hexahedral cells (the grid), and the solution will be obtained at each nodal point. The FDM is easiest to understand when the physical grid is Cartesian, but through the use of curvilinear transforms the method can be extended to domains that are not easily represented by brick-shaped elements. The Discretization results in a system of equation of the variable at nodal points, and once a solution is found, then we have a discrete representation of the solution.

5.3.2. FINITE ELEMENT METHOD (FEM)

FEM uses the simple piecewise functions valid on elements to describe the local variations of unknown flow variables. Governing equation is precisely satisfied by the exact solution of flow variables. The computational domain is divided up into smaller domains (finite elements) and the solution in each element is constructed from the basic functions. The actual equations that are solved are typically obtained by restating the conservation equation in weak form. The field variables are written in terms of the basic functions, the equation is multiplied by appropriate test functions, and then integrated over an element. Since the FEM solution is in terms of specific basis functions, a great deal more is known

about the solution than for either FDM or FVM. In FEM, residuals are used to measure the errors.

5.3.3. FINITE VOLUME METHOD (FVM)

A finite volume method (FVM) discretization is based upon an integral form of the PDE to be solved (e.g. conservation of mass, momentum, or energy). The PDE is written in a form which can be solved for a given finite volume (or cell). The computational domain is discretized into finite volumes and then for every volume, the 12 governing equations are solved.

The resulting system of equations usually involves fluxes of the conserved variable, and thus the calculation of fluxes is very important in FVM. The basic advantage of this method over FDM is it does not require the use of structured grids, and the effort to convert the given mesh in to structured numerical grid internally is completely avoided. As with FDM, the resulting approximate solution is a discrete, but the variables are typically placed at cell centers rather than at nodal points. This is not always true, as there are also face-centered finite volume methods. In any case, the values of field variables at non-storage locations (e.g. vertices) are obtained using interpolation.

5.3.4. SPECTRAL METHOD

Another method of generating a numerical analog of a differential equation is by using Fourier series or series of Chebyshev polynomials to approximate the unknown functions. Such methods are called the Spectral method.

Fourier series or series of Chebyshev polynomials are valid throughout the entire computational domain. This is the main difference between the spectral method and the FDM and FEM, in which the approximations are local. Once the unknowns are replaced with the truncated series, certain constraints are used to generate algebraic equations for the coefficients of the Fourier or Chebyshev series. Either weighted residual technique or a technique based on forcing the approximate function to coincide with the exact solution at several grid points is used as the constraint.

5.4. GOVERNING EQUATIONS IN CFD

Navier-Stokes equations are the governing equations of Computational Fluid Dynamics. It is based on the conservation law of physical properties of fluid. The principle of conservational law is the change of properties, for example mass, energy, and momentum, in an object is decided by the input and output. Applying the mass, momentum and energy conservation, we can derive the continuity equation, momentum equation and energy equation as follows.

CONTINUITY EQUATION

Continuity equation it is based on the principle of conservation of mass. Net mass flow out of control volume = time rate of decrease of mass inside control volume mass conservation equation.

$$\frac{D\rho}{Dt} + \rho \frac{\partial U_i}{\partial x_i} = 0 \tag{5.1}$$

MOMENTUM EQUATION

Momentum equation it is based on the law of conservation of momentum, which states that the net force acting in a fluid mass is equal to change in momentum of flow per unit time in that direction. The force acting on a fluid element mass "m" given by Newton's second law of motion is f = m * a where 'a' is the acceleration acting in the same direction as force - momentum equation.

$$\underbrace{\rho \frac{\partial U_j}{\partial t}}_{\text{i}} + \underbrace{\rho * U_i \frac{\partial U_j}{\partial x_i}}_{\text{ii}} = \underbrace{\rho * g_j}_{\text{iii}} - \underbrace{\frac{\partial P}{\partial x_j}}_{\text{iv}} - \underbrace{\frac{\partial \tau_{ij}}{\partial x_j}}_{\text{v}} \tag{5.2}$$

Where, $\tau_{ij} = -\mu * \left[\frac{\partial U_i}{\partial x_j} + \frac{\partial U_j}{\partial x_i}\right] + \frac{2}{3}\delta_{ij} * \mu * \frac{\partial U_k}{\partial x_k}$ (5.3)

i: Local change with time

ii: Momentum convection

iii: Mass force

iv: Surface force

v: Molecular-dependent momentum exchange (diffusion)

ENERGY EQUATION

Energy equation it is based on the principle that total energy is conserved. Total energy entering control volume = total energy leaving control volume energy equation.

$$\underbrace{\rho c_\mu \frac{\partial T}{\partial t}}_{\text{i}} + \underbrace{\rho c_\mu U_i \frac{\partial T}{\partial x_i}}_{\text{ii}} = \underbrace{-P \frac{\partial U_i}{\partial x_i}}_{\text{iii}} + \underbrace{\lambda \frac{\partial^2 T}{\partial x^2}}_{\text{iv}} - \underbrace{\tau_{ij} \frac{\partial U_j}{\partial x_i}}_{\text{v}} \quad (5.4)$$

i: Local energy change with time

ii: Convective term

iii: Pressure work

iv: Heat flux (diffusion)

v: Irreversible transfer of mechanical energy into heat

5.5. EXPLICIT VERSUS IMPLICIT METHODS

Numerical solution schemes are often referred to as being explicit or implicit. When a direct computation of the dependent variables can be made in terms of known quantities, the computation is said to be explicit. When the dependent variables are defined by coupled sets of equations, and either a matrix or iterative technique is needed to obtain the solution, the numerical method is said to be implicit.

In computational fluid dynamics, the governing equations are nonlinear, and the number of unknown variables is typically very large. Under these conditions implicitly formulated equations are almost always solved using iterative techniques.

Iterations are used to advance a solution through a sequence of steps from a starting state to a final, converged state. This is true whether the solution sought is either one step in a transient problem or a final steady-state result. In either case, the iteration steps resemble a time-like process. Of course, the iteration steps usually do not correspond to a realistic time dependent behaviour. In fact, it is this aspect of an implicit method that makes it attractive for steady-state computations, because the number of iterations required for a solution is often much smaller than the number of time steps needed for an accurate transient that asymptotically approaches steady conditions.

5.6. TURBULENCE MODELS:

In Reynolds averaging, the solution variables in the instantaneous (exact) Navier-Stokes equations are decomposed into the mean (ensemble-averaged or time-averaged) and fluctuating components. For the velocity components:

$$u_i = \overline{u}_i + u_i' \tag{5.5}$$

and the continuity equation:

$$\frac{D\rho}{Dt} + \rho \frac{\partial U_i}{\partial x_i} = 0 \tag{5.6}$$

where $\overline{u}_i$ and u_i' are the mean and fluctuating velocity components (i = 1,2,3).

Substituting expressions of this form for the flow variables into the instantaneous continuity and momentum equations and taking a time (or ensemble) average (and dropping the overbar on the mean velocity, $\overline{u}$) yields the ensemble-averaged momentum equations. They can be written in Cartesian tensor form as[13]:

$$\frac{\partial}{\partial t}(\rho u_i) + \frac{\partial}{\partial x_j}\left(\rho u_i u_j\right) = -\frac{\partial p}{\partial x_i} + \frac{\partial}{\partial x_j}\left[\mu\left(\frac{\partial u_i}{\partial x_j} + \frac{\partial u_j}{\partial x_i} - \frac{2}{3}\delta_{ij}\frac{\partial u_l}{\partial x_l}\right)\right] + \frac{\partial}{\partial x_j}\left(-\rho\overline{u_i' u_j'}\right) \tag{5.7}$$

5.6.1. K-Ɛ MODEL

The k-Ɛ model is a two-equation model, modeling both turbulent kinetic energy, k, and the dissipation, Ɛ. This is a complete model capable of calculating a turbulent flow without prior knowledge such as mixing length models. Standard models of k-Ɛ are so called "high Reynolds number models", meaning that wall functions are used to model the flow near the wall. Adaptations for the "low Reynolds number models" do exist however. The turbulent kinetic energy is derived for k-Ɛ by computing the partial derivative of k to time, the advection term, the turbulent transport, the dissipation and the production term[13].

$$\frac{\partial k}{\partial t} + \overline{u}\frac{\partial k}{\partial x_j} = \tau_{ij}\frac{\partial \overline{u}_i}{\partial x_j} - \epsilon + \frac{\partial}{\partial x_j}\left[\left(\nu + \frac{\nu_\tau}{\sigma_\kappa}\right)\frac{\partial k}{\partial x_j}\right] \tag{5.8}$$

And the rate of dissipation provides the value for Ɛ:

$$\frac{\partial \epsilon}{\partial t} + \overline{u}_j\frac{\partial \epsilon}{\partial x_j} = C_{\epsilon 1}\frac{\epsilon}{\kappa}\tau_{ij}\frac{\partial \overline{u}_i}{\partial x_j} - C_{\epsilon 2} * \frac{\epsilon^2}{\kappa} + \frac{\partial}{\partial x_j}\left[\left(\nu + \frac{\nu_\tau}{\sigma_\kappa}\right)\frac{\partial \epsilon}{\partial x_j}\right] \tag{5.9}$$

5.6.2. K-ω MODEL

The k−ω model replaces the equation for dissipation with one for specific dissipation rate ω, also expressed as Ɛ/k. The k −ω is also a closed model like the k −Ɛ model but unlike the k −Ɛ model it is inherently a "low Reynolds number" model, meaning that integration of every equation in the RANS model is carried out in every domain of the flow, including those near the wall. Though once again, "high Reynolds number" adaptations do exist. The expression for turbulent kinetic energy is slightly adapted, with closure coefficients β∗ and σ∗[13]:

$$\frac{\partial k}{\partial t} + \bar{u}_j \frac{\partial k}{\partial x_j} = \tau_{ij} \frac{\partial \bar{u}'_i}{\partial x_j} - \beta * k\omega + \frac{\partial}{\partial x_j}\left[(\nu + \sigma * k/\omega)\frac{\partial k}{\partial x_j}\right] \quad (5.10)$$

The expression for the specific dissipation rate is as follows:

$$\frac{\partial \omega}{\partial t} + \bar{u}_j \frac{\partial \omega}{\partial x_j} = \alpha \frac{\omega}{\kappa} \tau_{ij} \frac{\partial \bar{u}'_i}{\partial x_j} - \beta * \omega^2 + \frac{\sigma_d}{\omega} \frac{\partial k}{\partial x_j} \frac{\partial \omega}{\partial x_j} + \frac{\partial}{\partial x_j}\left[\left(\nu + \sigma * \frac{k}{\omega}\right)\frac{\partial \omega}{\partial x_j}\right] \quad (5.11)$$

For the k −ω model the kinematic eddy viscosity is expressed as follows:

$$\nu_\tau = \frac{\kappa}{\tilde{\omega}} \quad (5.12)$$

5.6.3. K−ω SHEAR STRESS TRANSPORT MODEL

The principle idea behind the SST models was to combine the best elements of the k-Ɛ and the k-ω. This was achieved by introducing functions which gradually blended the different elements of these models into a single formulation. Obviously, this is a pragmatic engineering approach, justified only by an improved model performance. It is to be explicitly stressed that the SST model owes much of its success to the robust and accurate near wall formulation.

Specifically, the combination means that k−ω is used close to the wall and k−Ɛ for the free stream flow, with the exact ratio being controlled by so-called blending factors and functions. By combining these models, the SST model manages to handle flows that feature strong pressure gradients without some of the downsides that plague k−ω. One of those is the sensitivity to farfield or freestream boundary conditions, The Shear Stress Transport part of the model refers to the fact that this model includes the transport term for the turbulent shear stress. This feature is only applied to the boundary layer of the flow[13].

5.7. PROCEDURE FOR CFD ANALYSIS

During preprocessing, the geometry of the problem can be defined. From there, data can be suitably processed and the fluid volume (or fluid domain) is extracted. The volume occupied by the fluid is divided into discrete cells (the mesh). The mesh is structured, consisting of a combination of hexahedral and tetrahedral. The physical modeling is defined. Boundary conditions are defined. This involves specifying the fluid behavior and properties at all bounding surfaces of the fluid domain.

The simulation is started and the equations are solved iteratively as a steady-state. Finally, a postprocessor is used for the analysis and visualization of the resulting solution.

5.7.1. MESHING

The finite volume method (FVM) is a common approach used in CFD codes, as it has an advantage in memory usage and solution speed, especially for large problems, high Reynolds number turbulent flows. In the finite volume method, the governing partial differential equations are recast in a conservative form, and then solved over discrete control volumes. This discretization guarantees the conservation of fluxes through a particular control volume.

The required mesh size is defined and various steps are performed to produce a mesh of high quality. Grid angles are exceptionally good, mesh sizes transition smoothly, and high aspect-ratio elements are generated in the near-wall regions to resolve these regions efficiently and capture boundary layer and recirculation zone accurately.

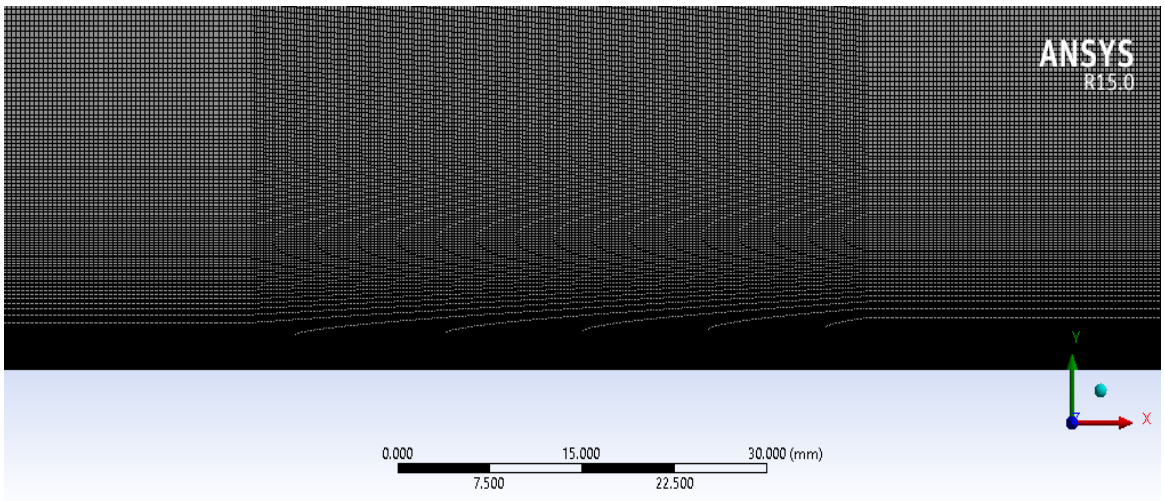

Fig 5.1. Cut section of the 2-D Meshed Model

Table 5.1 2-D Mesh Properties

PARAMETERS	FINE MESH
No. of elements	620400
No. of nodes	1864842
Physics Preference	CFD
Solver Preference	Fluent
Type of mesh	Quad-8
Relevance center	Fine
Initial size seed	Active assembly
Smoothing	High
Span angle center	Fine
Curvature normal angle	30.0*
Min size	3.177 mm
Max face size	15.885 mm
Growth rate	1.2 (default)
Mini edge length	0.0249 mm
Mesh Metric	Skewness
Minimum	1.3057293e-10
Maximum	0.2146154
Average	4.4912757e-02
Standard deviation	6.5265068e-02

The total geometry shown in the fig. 5.2 is divided into several blocks of different sizes. The block size is smaller between the wedge and the flat plate where the whole shockwave boundary layer interaction phenomena occurs and larger blocks are made in the rest of the domain. The whole domain is divided into a total of 49 blocks out of which 47 are cuboids and 2 are with triangular face.

All the cuboids are given edge sizing with respect to block dimensions i.e., 2/3th of the block edge length. The remaining 2 triangular faced blocks are given body sizing of 1mm and 3mm which are near to the wedge and the plate respectively.

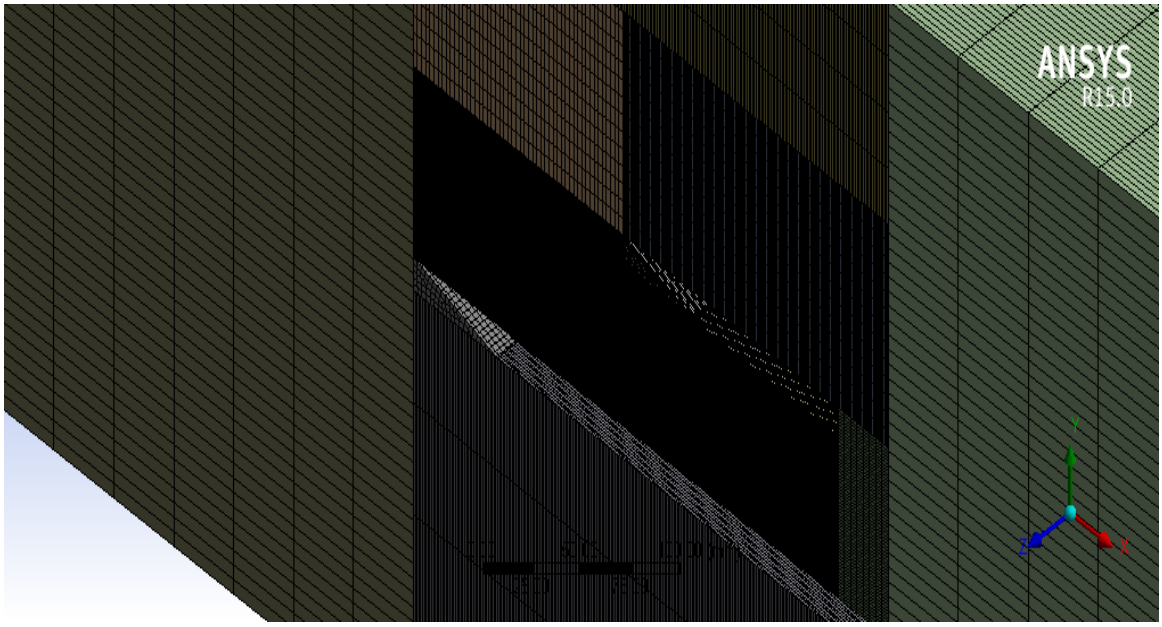

Fig. 5.2. Meshing pattern is seen with 25,58,000 grid elements and 28,73,000 nodes.

5.7.2. PREPROCESSING

After finishing the meshing process, ANSYS-Fluent boundary conditions are defined.

Table 5.2 Preprocessing Parameters

DOMAIN	AIR
Model	Density based Energy equation ON SST K omega turbulence model
Material	Ideal gas Viscosity (Sutherland law) Specific Heat = 1006.43 J/kg-K
Boundary Condition	Inlet: Velocity inlet Velocity = 523 m/s Inlet gauge pressure = 24650 pascal Inlet StaticTemperature = 161.9125 K Outlet: Pressure outlet Gauge pressure = 0 pascal Wall: No-slip condition
Solution method	Explicit
Solution controls	Courant No = 0.5
Solution initialization	Standard initialization

5.7.3. ANALYSIS

The file is solved in CFD – Fluent for the input boundary conditions as given. This solver uses RANS equations to solve for required parameters. Residual criteria are given as 10^{-8}. Typical convergence residual graph is shown.

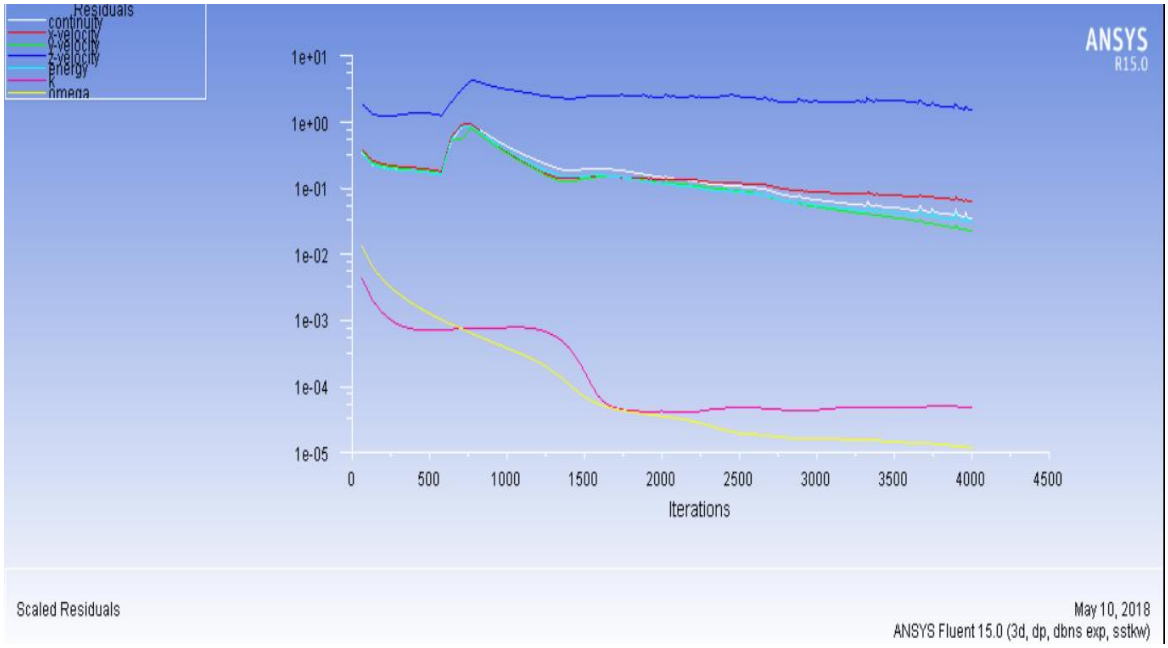

Fig. 5.3. Scaled Residuals Plot

5.7.4. POST PROCESSING

Parameters like Pressure, Velocity, Temperature, Mach Number and Boundary Layer thickness are obtained at various locations in the domain. Shock Impingement Location, Flow Separation Location, Flow Reversal Location, Interaction Length are measured. The contours and vector plots of Pressure and Velocity are visualized.

5.8. GRID INDEPENDENCE ANALYSIS

Grid dependency study is an essential part of the computational exercise by which discretization error can be minimized to get consistent and stable values. Grid convergence is the term used to describe the improvement of results by using successively smaller cell sizes for the calculations. A calculation should approach the correct answer as the mesh becomes finer, hence the term grid convergence.

The examination of the spatial convergence of a simulation is a straight-forward method for determining the ordered discretization error in a CFD simulation. The method

involves performing the simulation on two or more successively finer grids. The term grid convergence study is equivalent to the commonly used term grid refinement study.

The analysis is carried out for grid elements of 1058000, 2558000 and 5201000 of coarse, medium and fine mesh.

Table 5.3 Mesh Properties for 3-D (Without RVG)

PARAMETERS	COARSE	MEDIUM	FINE
No. of elements	1058000	2558000	5201000
No. of nodes	1233000	2873000	5690000
Physics Preference	CFD	CFD	CFD
Solver Preference	Fluent	Fluent	Fluent
Type of mesh	Hexahedron and Tetrahedron cells	Hexahedron and Tetrahedron cells	Hexahedron and Tetrahedron cells
Relevance center	Coarse	Medium	Fine
Initial size seed	Active assembly	Active assembly	Active assembly
Smoothing	High	High	High
Transition	Slow	Slow	Slow
Span angle center	Fine	Fine	Fine
Curvature normal angle	18.0*	5.0*	5.0*
Min size	0.51923 mm	0.152070 mm	0.152070 mm
Max face size	51.923 mm	15.2070 mm	15.2070 mm
Max size	103.85 mm	30.415 mm	30.415 mm
Growth rate	1.2 (default)	1.15	1.15
Mini edge length	4.5 mm	4.5 mm	4.5 mm
Mesh Metric	Skewness	Skewness	Skewness
Minimum	1.30572936 E-10	1.30572936 E-10	1.30572936 E-10
Maximum	0.7666812	0.7666679	0.7666672
Average	1.29858738 E-03	2.3427419 E-03	1.2347397 E-03
Standard deviation	1.84735018 E-02	2.1619813 E-02	1.5799478 E-02

CHAPTER-6

RESULTS AND DISCUSSION

CFD analysis has been carried out for 2-D and 3-D – with and without flow control devices. Results of each value has been studied and plotted. It will further be discussed in detail.

6.1. 2-D ANALYSIS RESULTS

6.1.1. STATIC PRESSURE VARIATION

Fig. 6.1. shows the pressure variation across the incident shock and reflected shock. It is observed that pressure increases across an incident oblique shock and decreased through expansion fan. The flow is again compressed by a coalesced series of compression waves

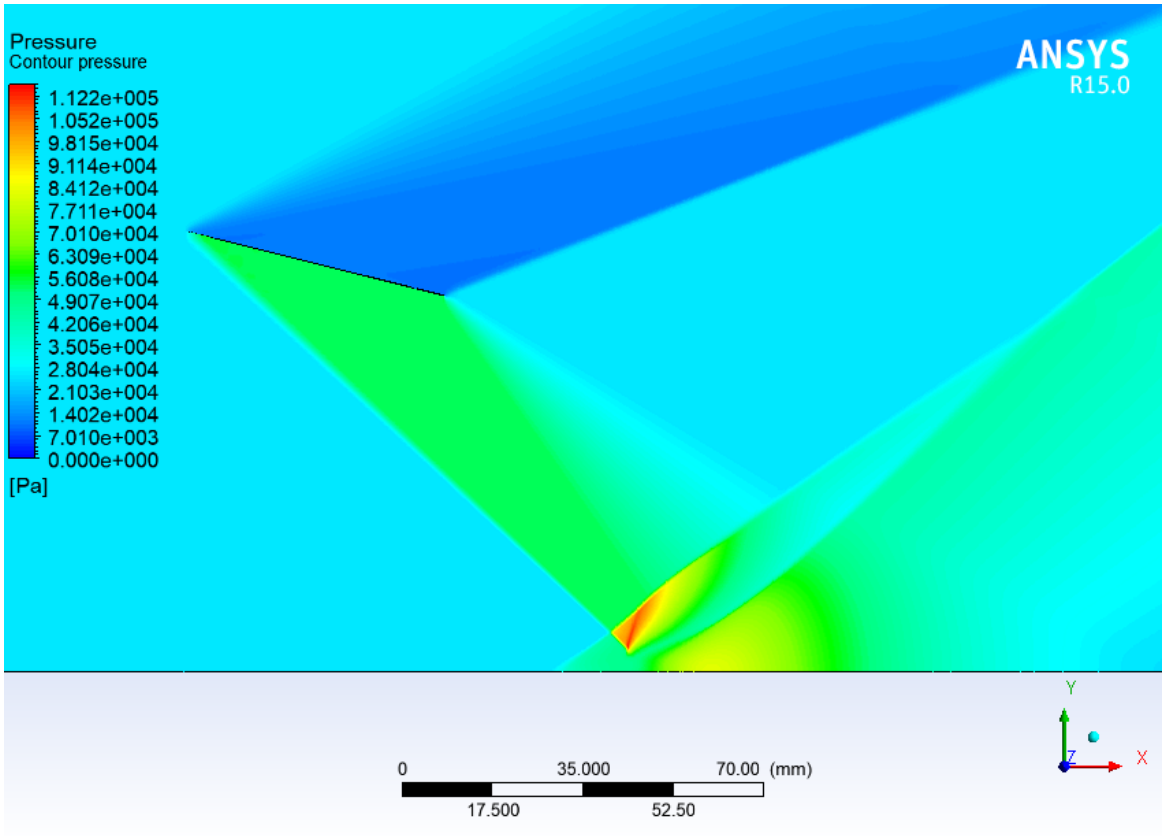

Fig. 6.1. Pressure Contour at Freestream Mach number 2.05

6.1.2. VELOCITY VARIATION

Figure shows that decrement in the velocity across the incident oblique shock wave. The recirculation zone is viewed in which the Mach number is of subsonic range.

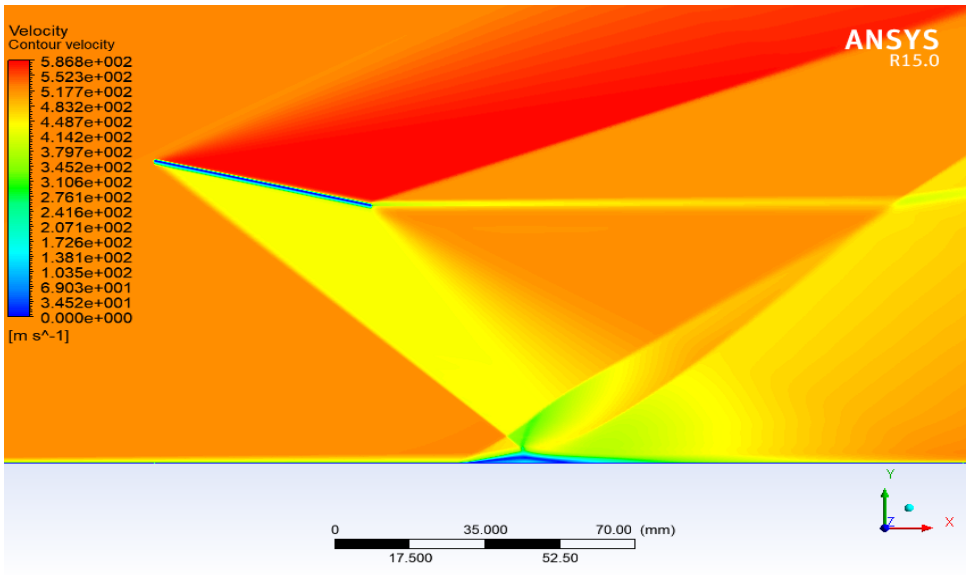

Fig. 6.2. Velocity contour at freestream Mach number 2.05

6.1.3. RECIRCULATION ZONE

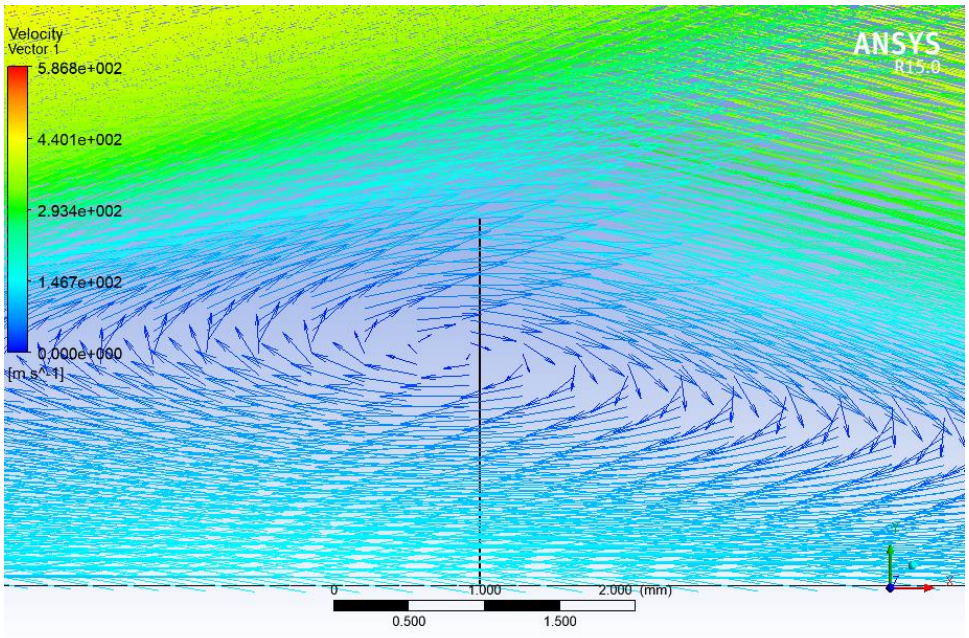

Fig. 6.3. Recirculation Zone

Fig. 6.3. shows the zoomed in velocity vector plot to view the recirculation zone where it is observed that velocity reduces to subsonic range at the near wall flow regime due to the low momentum boundary layer.

6.1.4. VALIDATION CASE

Figure 6.4 shows the Pressure ratio vs Normalized plate length plot from CFD which is validated with the help of the raw experimental data [1].

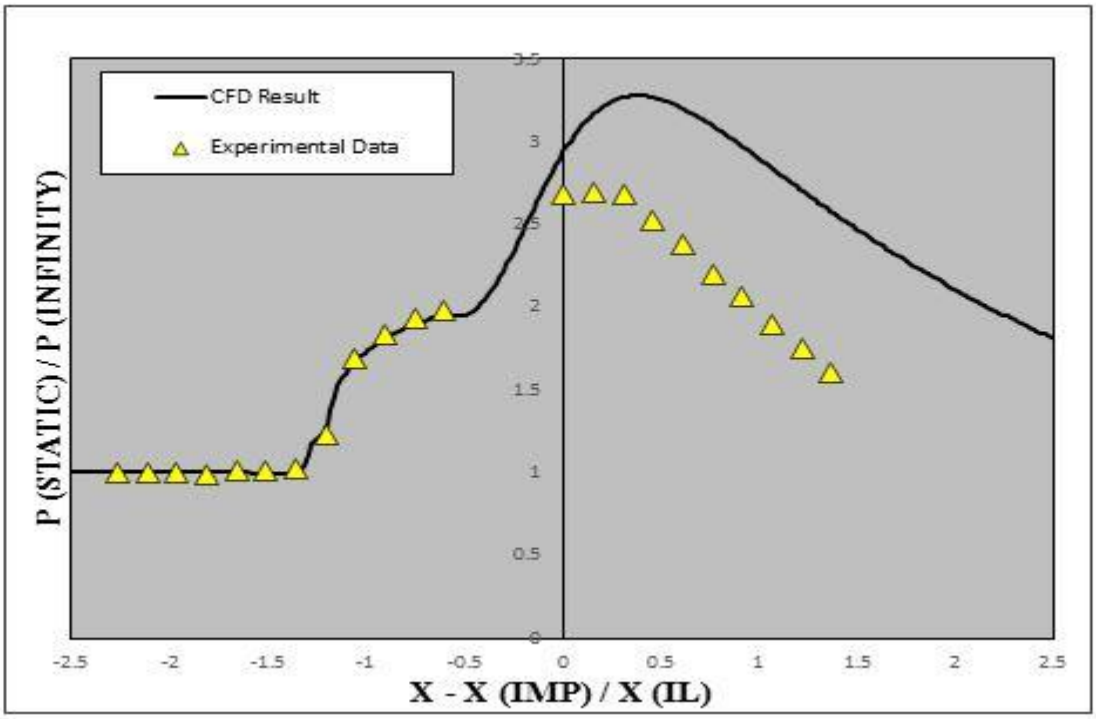

Fig. 6.4. Normalized Pressure Ratio plot for CFD Results and Experimental Data

6.1.5. PARAMETRIC ANALYSIS

Contours of velocity and pressure at various freestream Mach Number are discussed here. Formation of Mach Stem is observed at lower Mach Number which gradually disappears as the Mach Number increases.

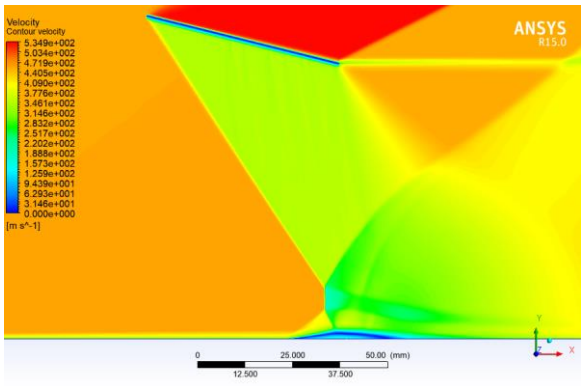

Fig. 6.5.1. M=1.65

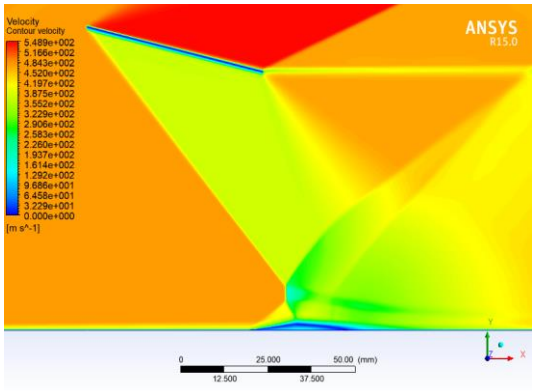

Fig. 6.5.2. M=1.75

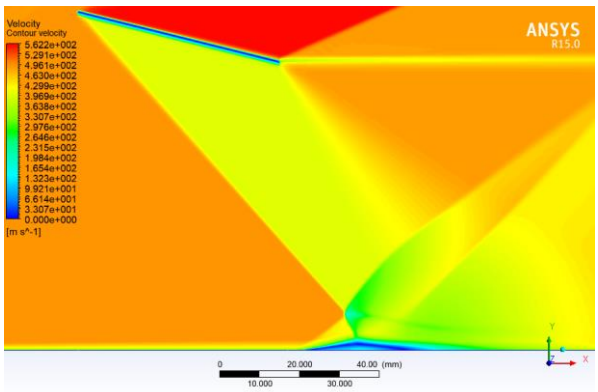

Fig. 6.5.3. M=1.85

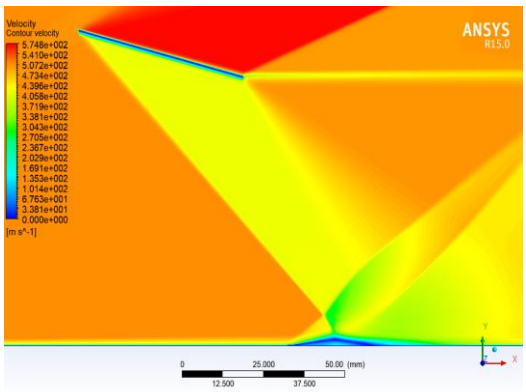

Fig. 6.5.4. M=1.95

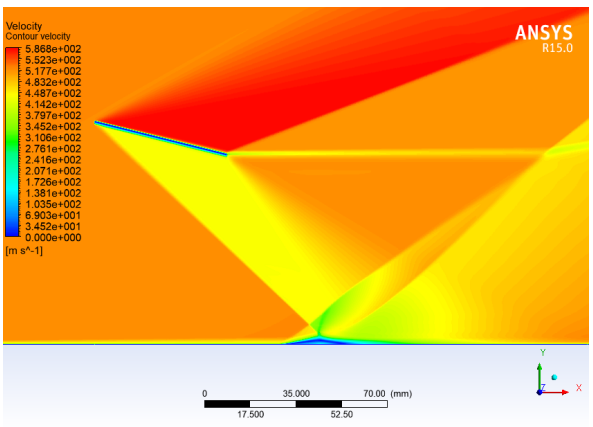

Fig. 6.5.5. M=2.05

Fig. 6.5. Velocity Contours for Various Mach Numbers

Fig.6.6. shows that the Maximum Pressure Ratio increases with the Mach number and the Separation point shifts downstream.

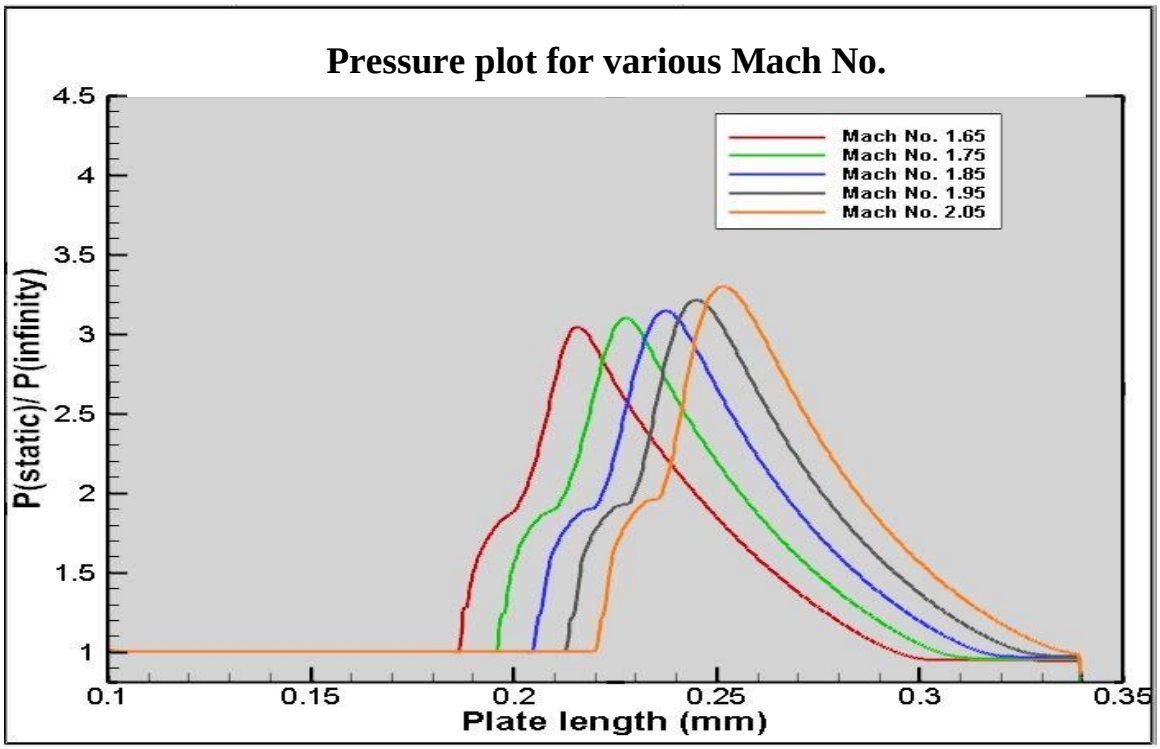

Fig. 6.6. Pressure Ratio vs Plate Length for Various Freestream Mach Numbers

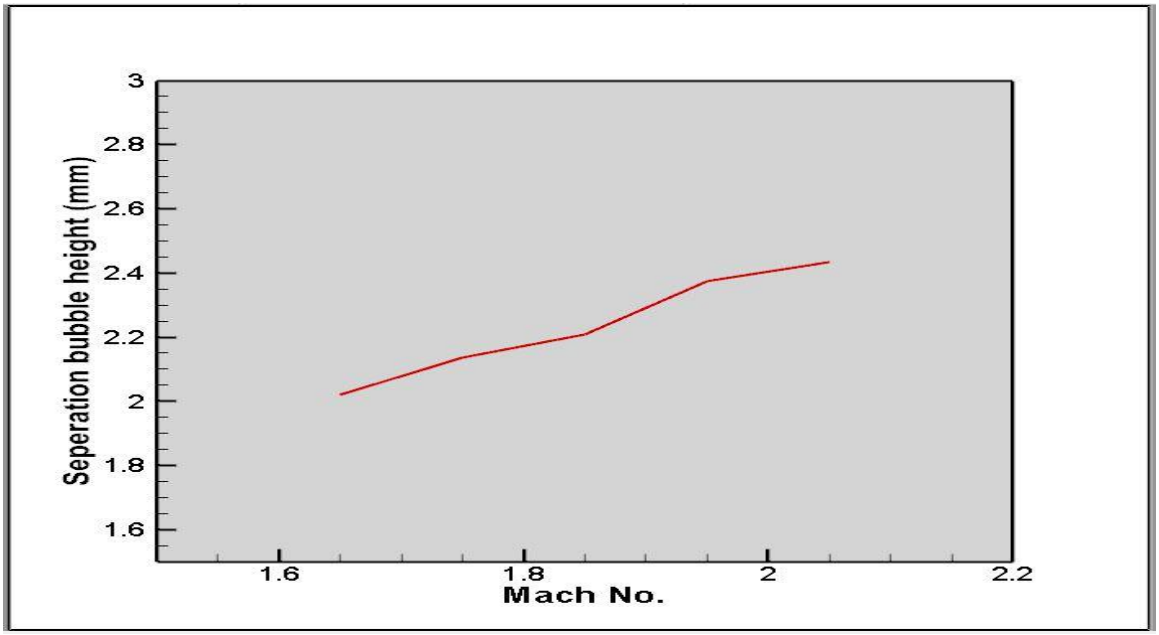

Fig. 6.7. Variation of Recirculation zone height with respect to Mach Number

Fig.6.7. shows that the recirculation zone height increases with the increase in Mach Number.

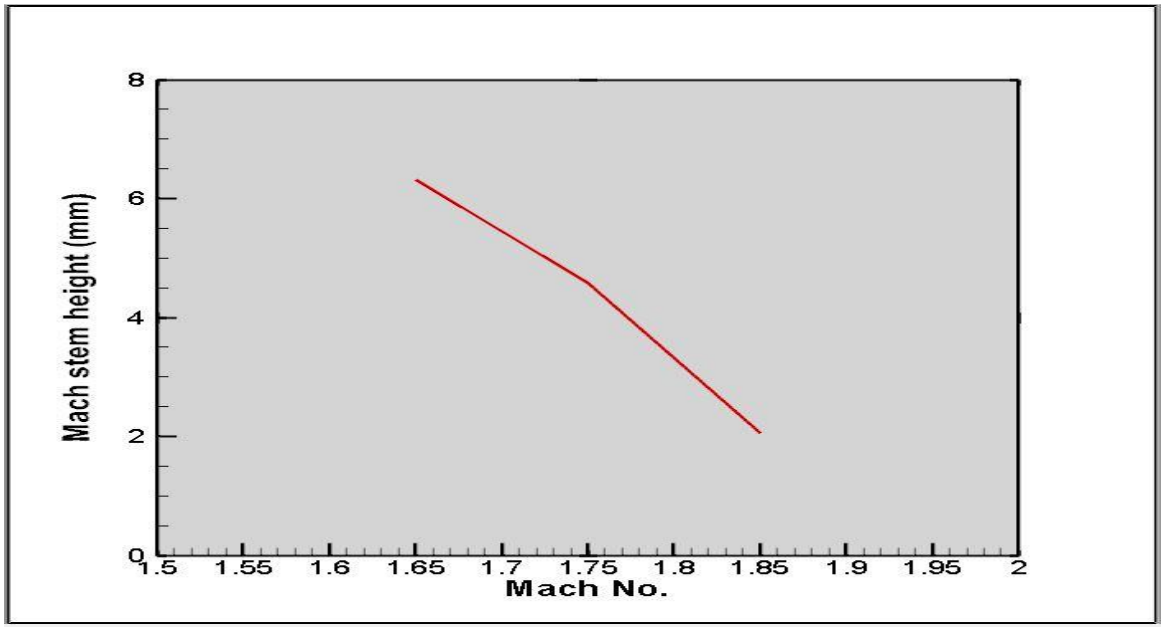

Fig. 6.8. Variation in Mach Stem Height with respect to Mach Number

Table 6.1 2-D Parametric Analysis Results

PARAMETERS	M_1=1.65	M_1=1.75	M_1=1.85	M_1=1.95	M_1=2.05
M_2	1.091	1.229	1.3268	1.4255	1.8323
V_2 (m/s)	338.23	372.377	393.69	414.749	434.07
β (degrees)	56.625	52.55	48.858	45.72	43.75
X_{imp} (mm)	205.859	215.876	225.153	232.354	239.966
X_s (mm)	188.209	197.975	206.576	213.705	221.7
X_{IL} (mm)	17.65	17.9	18.577	18.649	18.266
δ_1 (mm) wedge L.E	2.1	2.2	2.1	2.1	2.1
δ_2 (mm) wedge T.E	Flow reversal	Flow reversal	2.7	2.6	2.7
δ_s (mm)	2.4	2.6	2.7	2.7	2.9
H_B (mm)	2.02	2.1368	2.2068	2.375	2.434
H_m (mm)	6.314	4.577	2.055	-	-

6.2. 3-D ANALYSIS RESULTS WITHOUT RVG

6.2.1. STATIC PRESSURE VARIATION

Fig.6.9. shows the Pressure distribution across the mid-plane of the domain. The curvature of the separation line in Fig.6.10. indicates the pressure losses due to 3-D relieving effects at the plate edges.

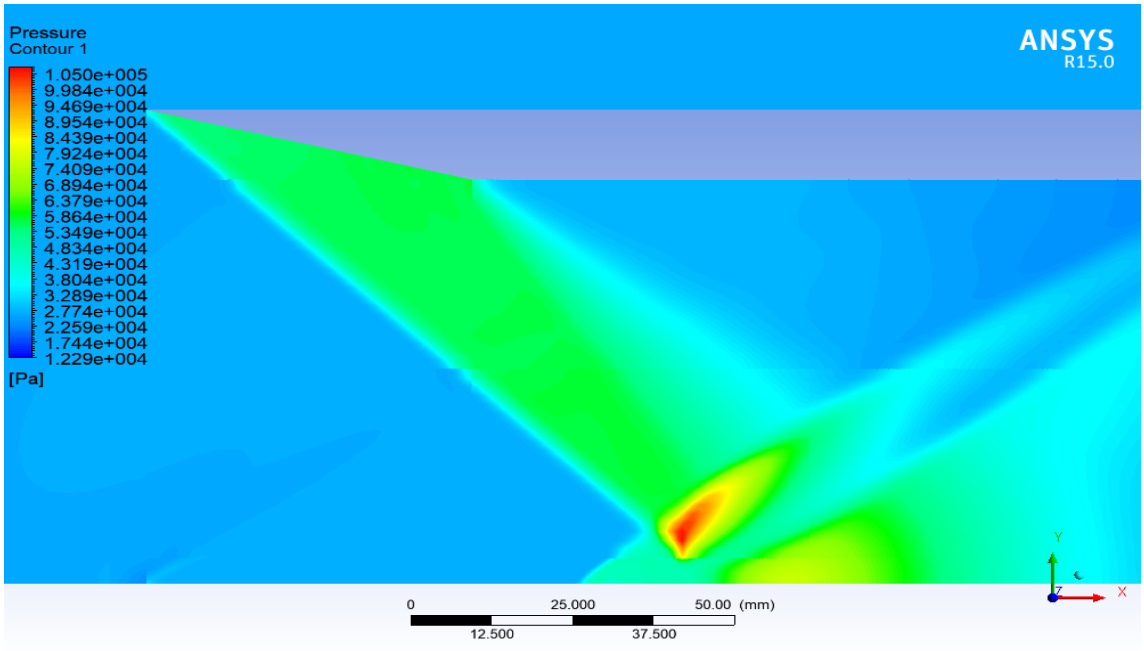

Fig. 6.9. Pressure Contour for freestream Mach Number 2.05

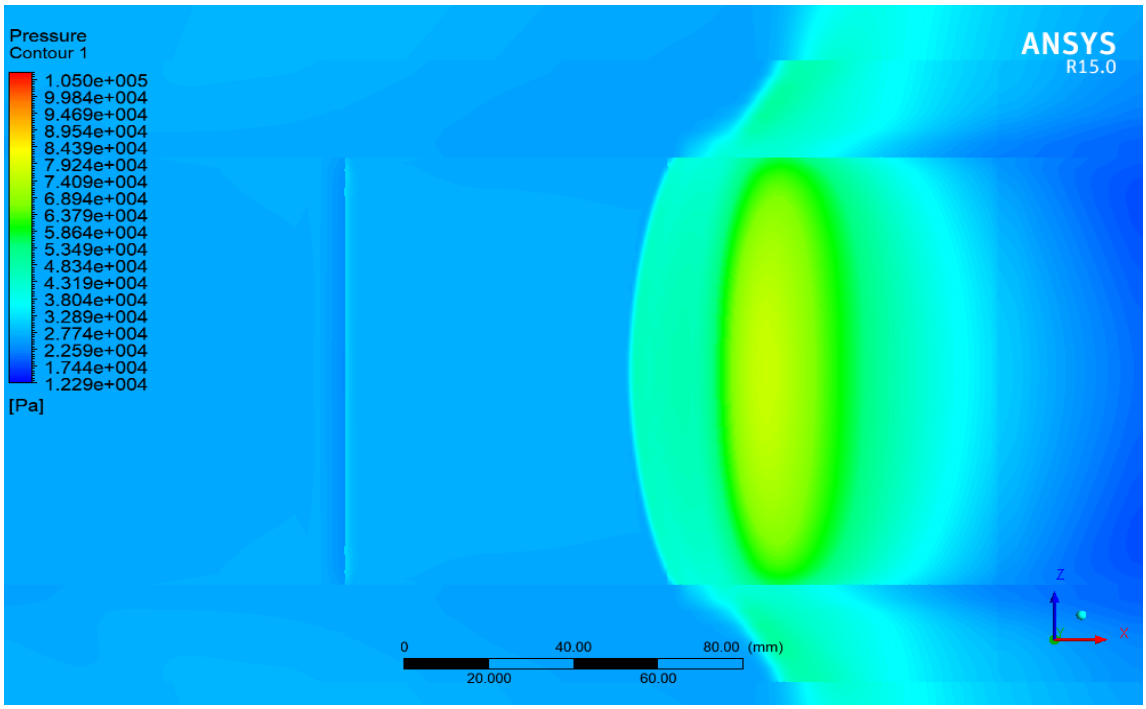

Fig. 6.10. Pressure Variation on Plate surface

6.2.2. VELOCITY VARIATION

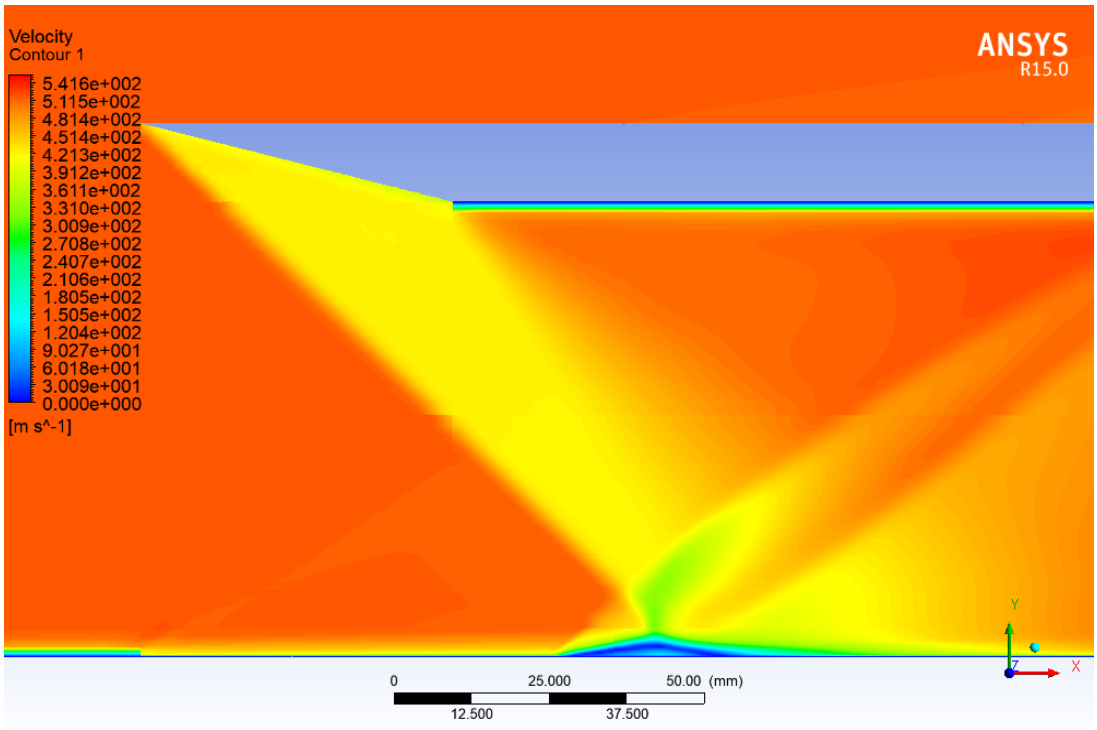

Fig. 6.11. Velocity Contour for Freestream Mach Number 2.05

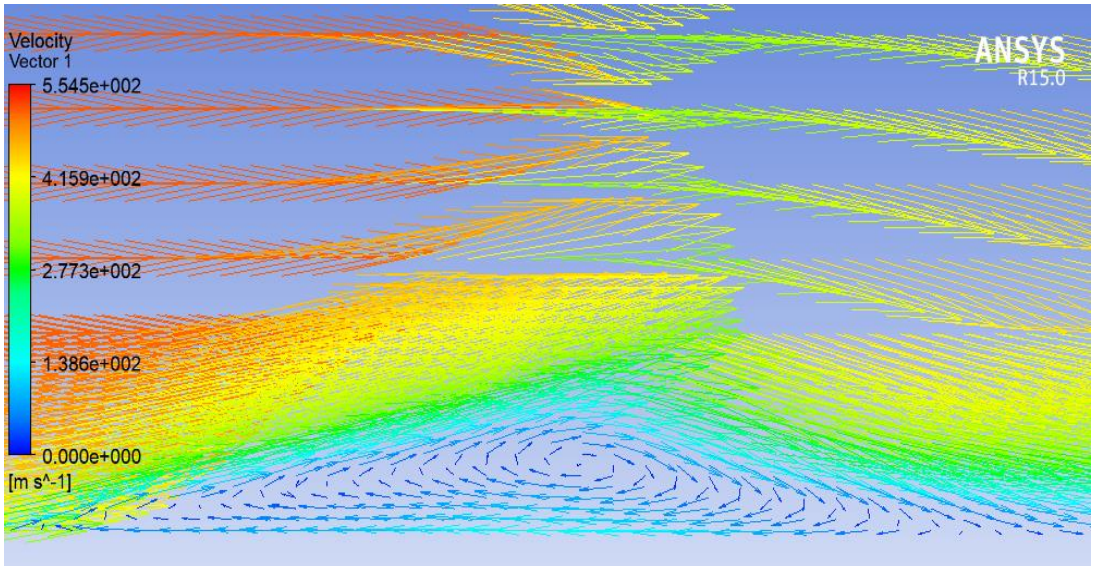

Fig. 6.12. Recirculation Zone for Freestream Mach Number 2.05

Fig.6.11. shows the Velocity Contour along with the small recirculation zone at the bottom in blue colour. The Vector Contour of zoomed recirculation zone is shown in Fig.6.12. and vector direction shows direction of flow.

Fig. 6.13. shows the pressure ratio plot for coarse, medium and fine mesh. And it is observed that the locations of pressure rise are appropriate and constant in the case of medium and fine mesh, so the medium mesh case is considered for the analysis to cut down the computation time.

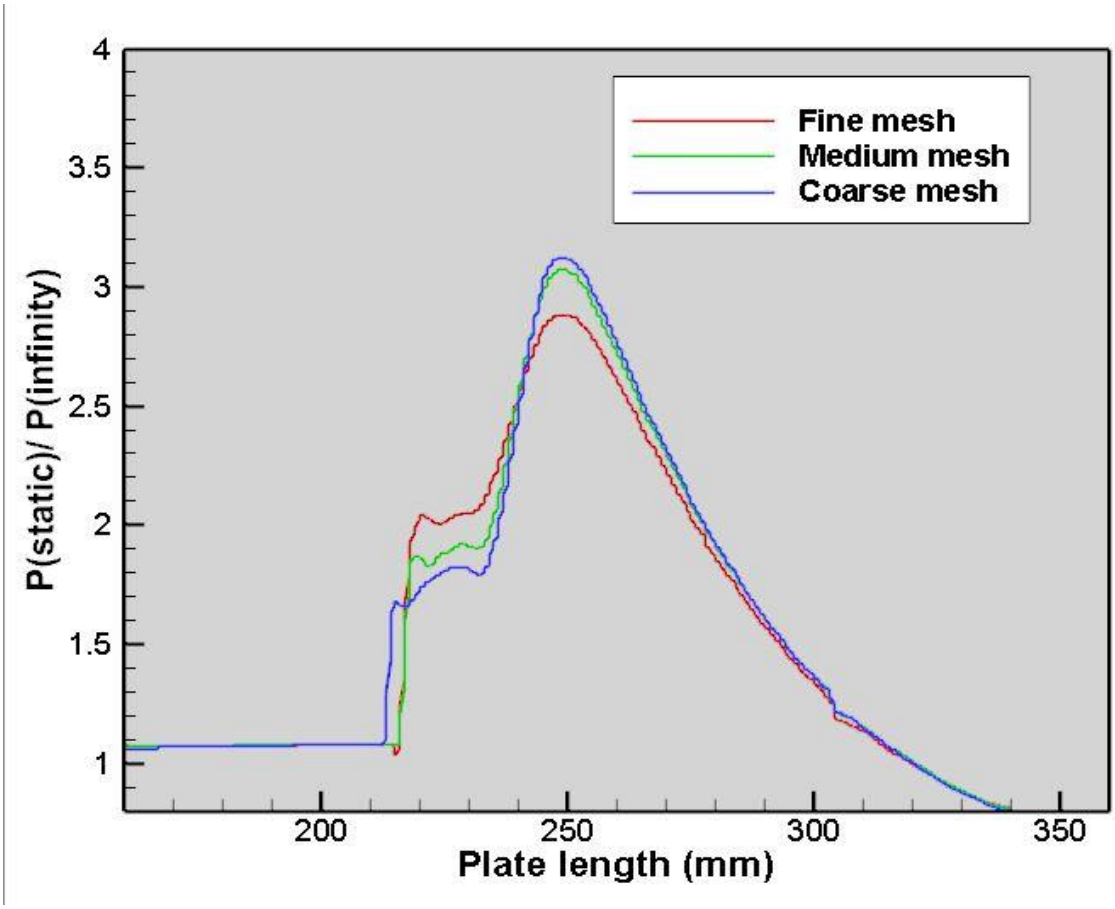

Fig. 6.13. Variation of $\frac{P_s}{P_\infty}$ Vs Plate Length for different mesh qualities

Table 6.2 Output Parameters for 3-D Analysis Without RVG

PARAMETERS	COARSE	MEDIUM	FINE
M_2	1.5028	1.504	1.5047
V_2 (m/s)	428.935	429.303	429.487
β (degrees)	43.83	43.74	43.91
X_{imp} (mm)	237.753	238.344	238.257
X_s (mm)	215.563	215.223	212.508
X_{IL} (mm)	22.189	23.121	25.749
δ_1 (mm) wedge L.E	4.5	4.2	4.2
δ_2 (mm) wedge T.E	4.2	4.4	4.4
δ_s (mm)	4.2	4.5	4.5
H_B (mm)	2.70446	2.732	2.746

Table 6.3 Percentage Error for 3-D Results for various Mesh Qualities without RVG

ACTUAL VALUES	COARSE	MEDIUM	FINE
M_2 = 1.53	1.778 %	1.699 %	1.653 %
β (degrees) = 42.93	2.09 %	1.907 %	2.28 %

6.3. 3-D ANALYSIS RESULTS WITH RVG

6.3.1. STATIC PRESSURE VARIATION

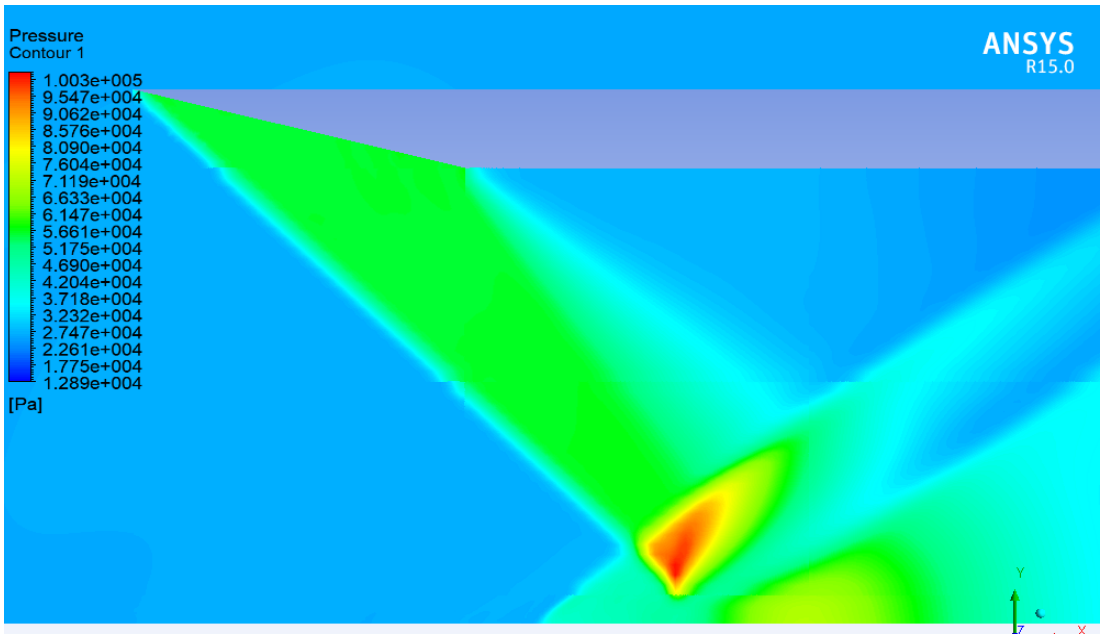

Fig. 6.14. Pressure Contour with RVG for freestream Mach Number 2.05

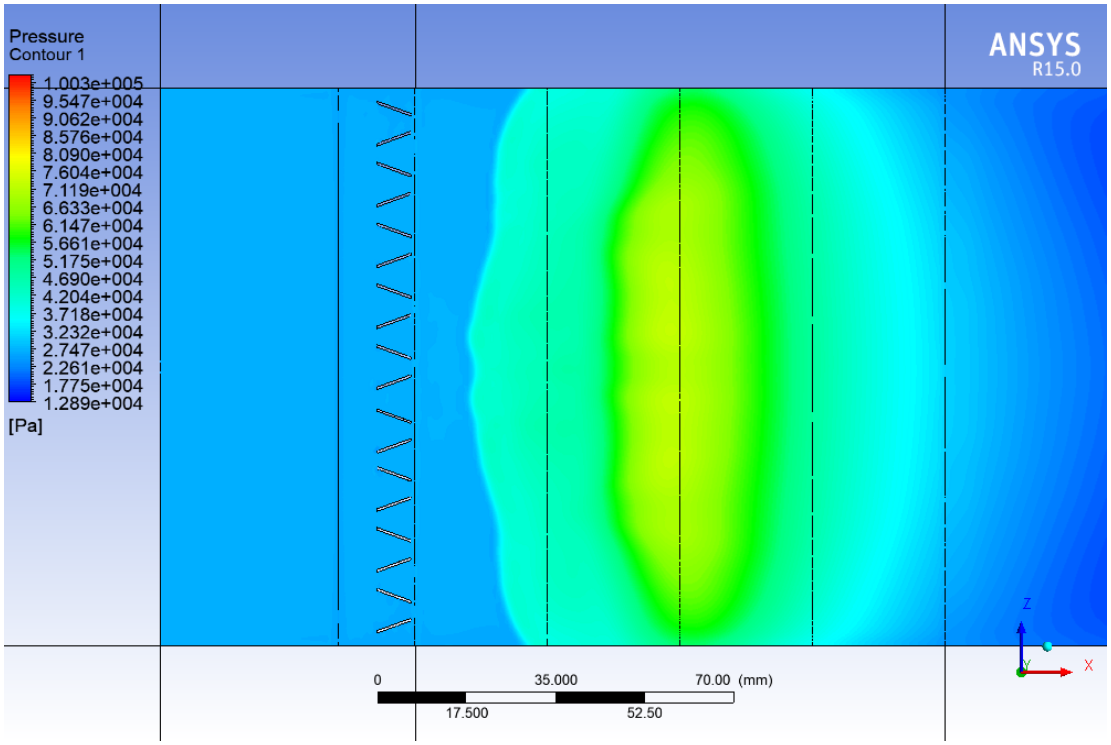

Fig. 6.15. Pressure Contour with RVG on Plate Surface

Fig 6.15 shows the Pressure Contour on plate surface and corrugation patterns in the separation line after employing RVGs.

6.3.2. VELOCITY VARIATION

The RVG induces spanwise variations in the form of corrugations in the separation line, caused due to the counter-rotating streamwise vortices interacting with the reversed flow in the recirculation zone fig.6.16(a).

A well-defined striation pattern downstream of the reattachment location is observed, which gives an idea about the impressions the counter-rotating vortices on the entire interaction fig.6.16(b).

The striation downstream of flow reattachment is formed exactly in the line along the center of each inter-device spacing of the RVGs fig.6.16(c).

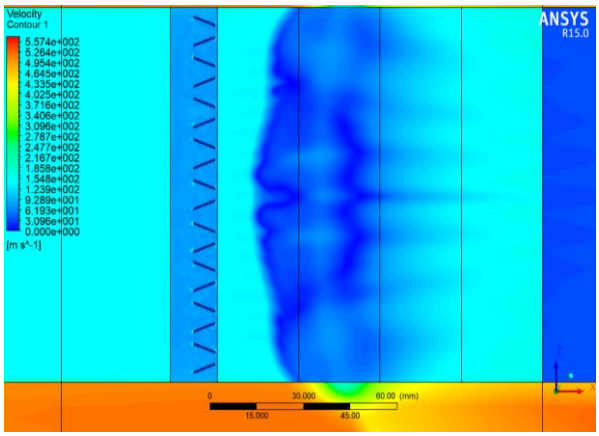

(a) Height=0.01mm

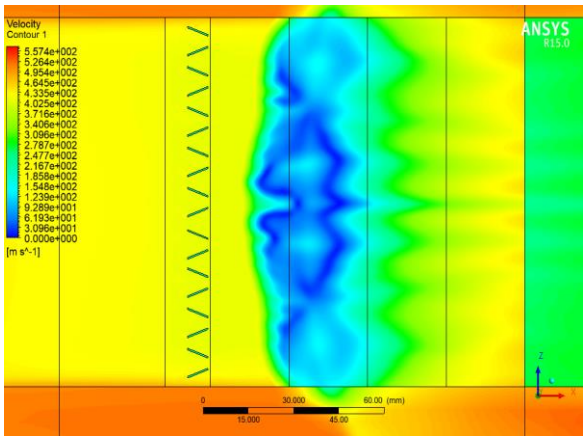

(b) Height=0.85mm

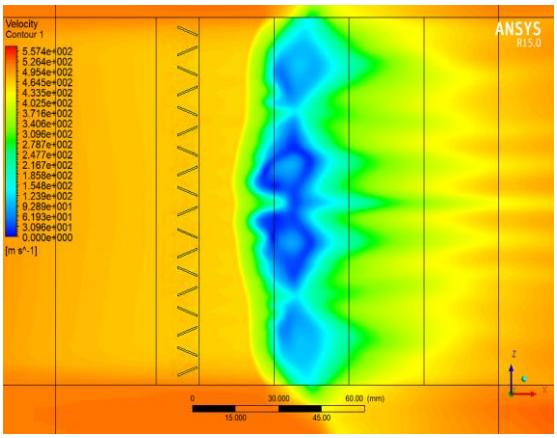

(c) Height=1.7mm

Fig. 6.16. Velocity Contours for Various Offset Planes from Plate surface

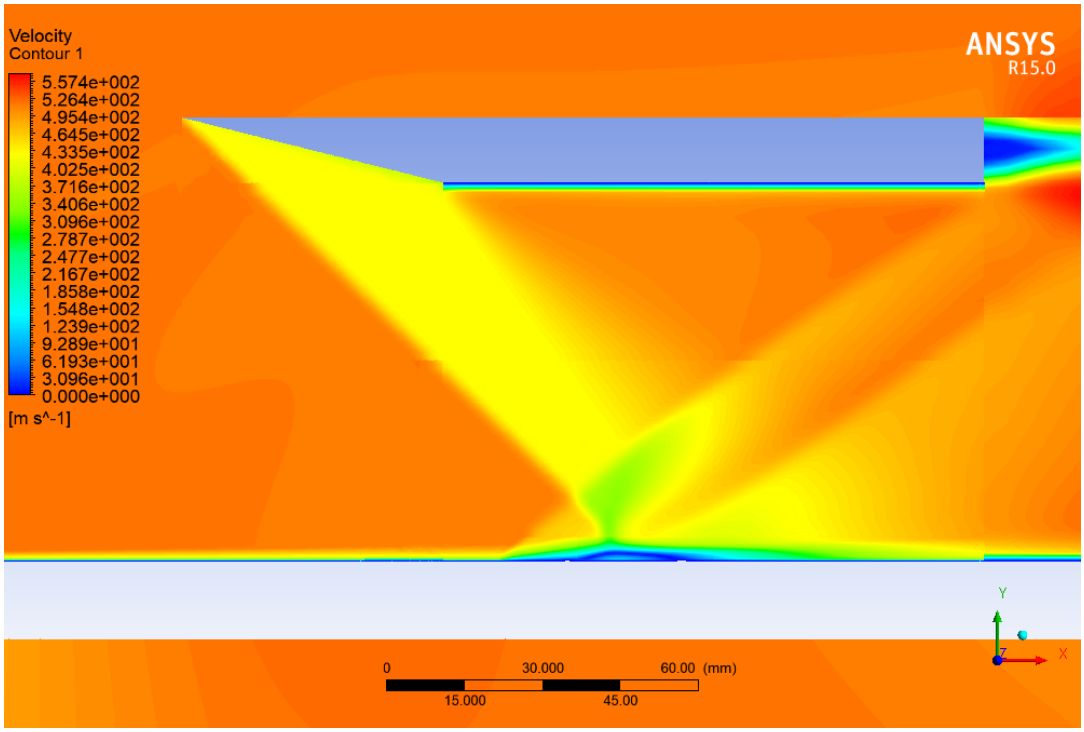

Fig. 6.17. Velocity Contour with RVG for freestream Mach Number 2.05

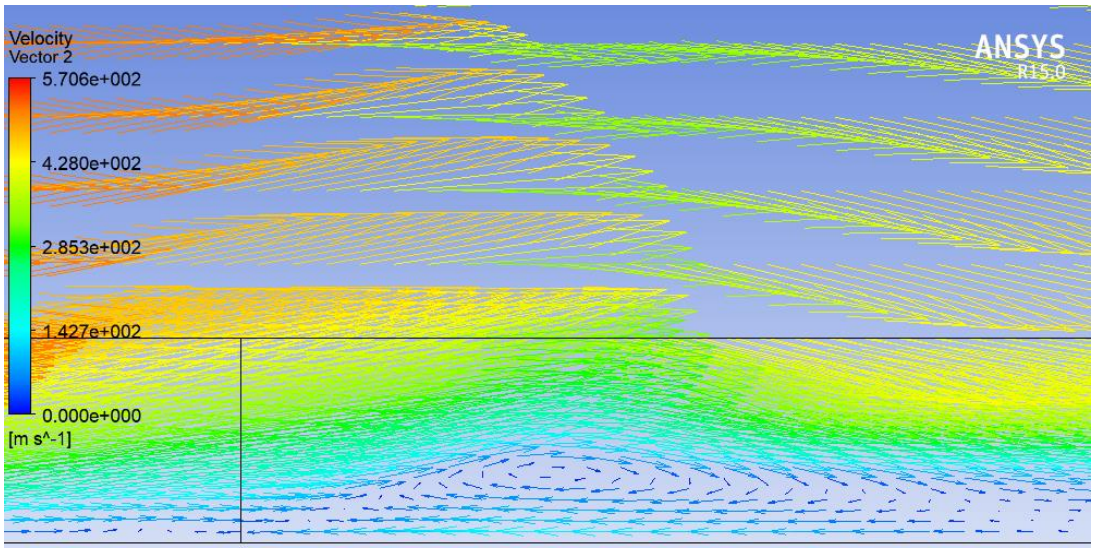

Fig. 6.18. Recirculation Zone with RVG for Freestream Mach Number 2.05

After implementing the RVGs, it has been observed that the recirculation zone has been pushed downstream due to the interaction of vortices with the separation line.

Table 6.4 Output Parameters for 3-D Analysis

PARAMETERS	WITH OUT VG	WITH VG h/ δ=0.378
M_2	1.504	1.5108
V_2 (m/s)	429.303	431.224
β (degrees)	43.74	44.23
X_{imp} (mm)	238.344	237.186
X_s (mm)	215.223	209.205
X_{IL} (mm)	23.121	27.981
δ_1 (mm) wedge L.E	4.2	2.5
δ_2 (mm) wedge T.E	4.4	3.3
δ_s (mm)	4.5	3.6
H_B (mm)	2.732	2.1047

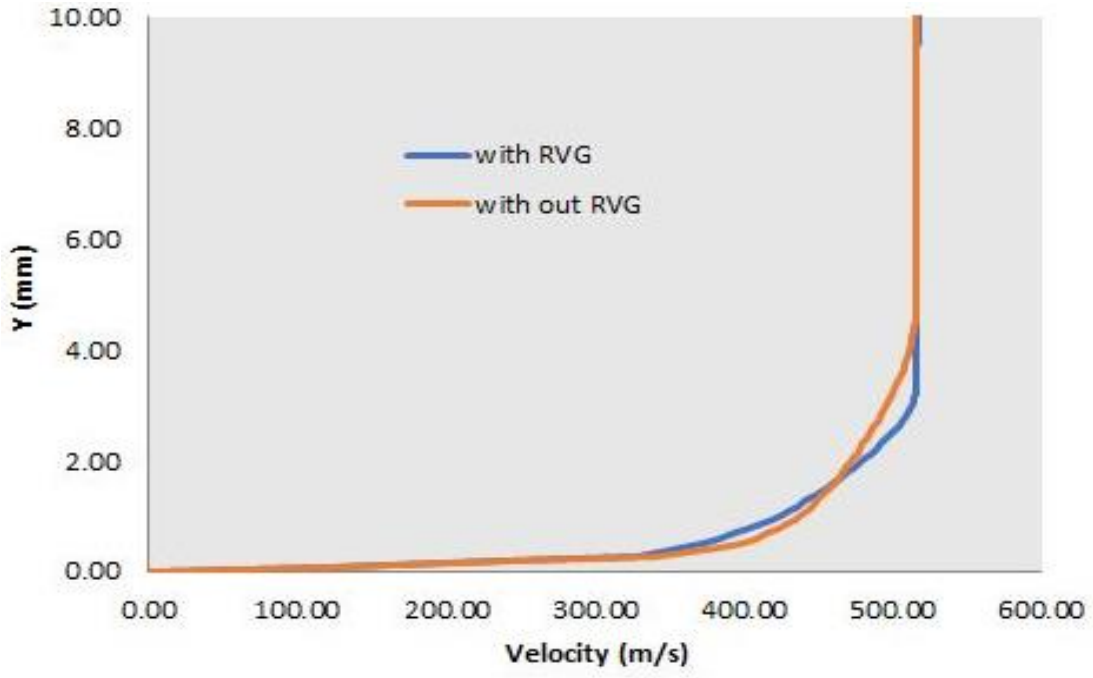

Fig. 6.19. Boundary Thickness for RVG and No-RVG cases

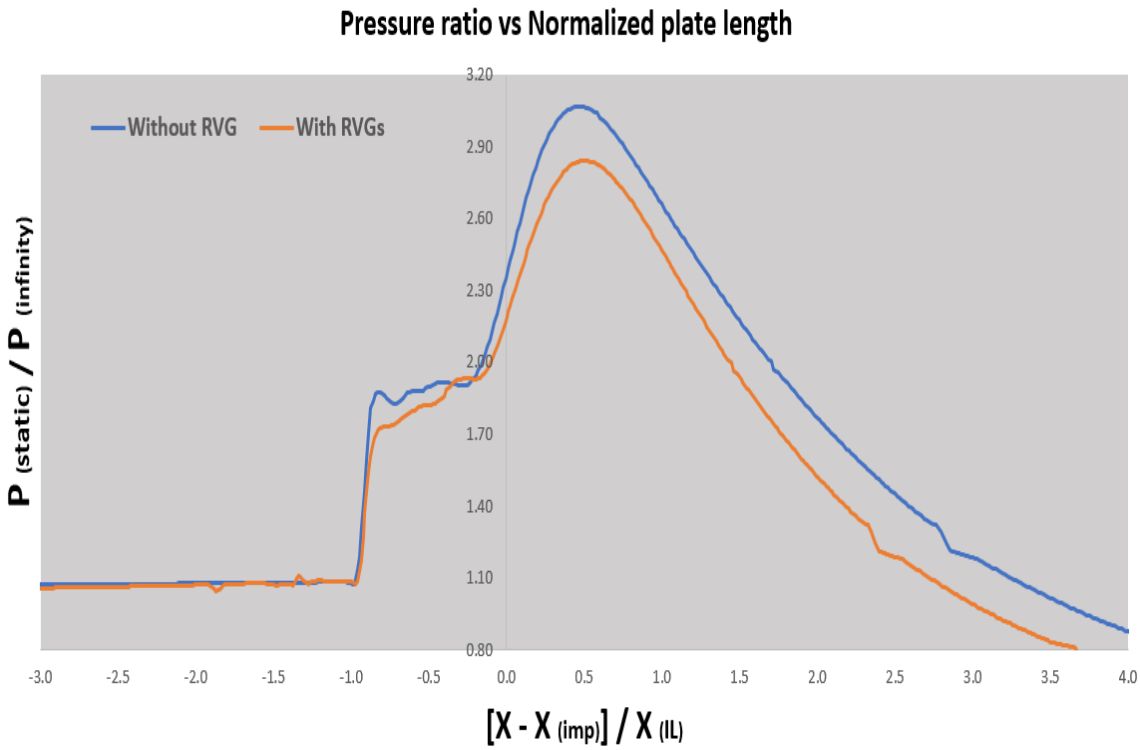

Fig. 6.20. Pressure Ratio plots for RVG and No-RVG case

Fig 6.20 shows comparison between Pressure Ratio plots for RVG and No- RVG case. Reduction in first and second pressure ratio can be seen which a direct measure of reduction in Shock- Foot unsteadiness.

Table 6.5 Influence of RVGs on various parameters

PARAMETERS	NO RVGs	RVGs	REDUCTION
H_B	2.732	2.1047	22.96 %
δ	4.5	3.6	20 %
P_s / P_∞	3.07	2.84	7.4918 %

CHAPTER-7

CONLUSION AND FUTURE SCOPE

7.1. CONCLUSION

Numerical investigations were carried out to study the shockwave boundary layer interactions on a flat plate of 2-D and 3-D cases for a freestream Mach number of 2.05. Wedge of a flow turning angle 14˚ was used to generate the incident shock wave over the flat plate. The effect of variation in freestream Mach number on the recirculation zone thickness is studied. The analysis was carried out for with and without RVG cases. Also, assessment of the effectiveness of the Micro Rectangular Vane Type Vortex Generators in controlling shock induced separation in flow of freestream Mach number 2.05 is studied. The RVG height spanned 37.78% of the local BLT of no-RVG case. Array of RVGs is placed at 5.5δ upstream of the separation location of no-RVG case. Following are the conclusions drawn from the present study:

- The parametric study revealed that the Maximum Pressure Ratio increases with the Mach number and the Separation point shifts downstream.
- The Recirculation Zone height increases with Mach Number because the shock deflection angle reduces leading to reduction in shock strength.
- The Mach steam length decreases with increasing Mach Number and eventually disappears.
- The separation point is shifted 2.796% (1.34δ) downstream with respect to the separation point for no control case.

7.2. SCOPE FOR FUTURE WORK

The parametric study on the passive device if extended for various Mach numbers will reveal the overall effectiveness of the device at different flight conditions. The height of the passive device is maintained as 0.378δ for the currently study, it will be interesting to study the variation in the height of the passive device. It is not clear what will be the net change in effectiveness if both the active and passive device are implemented in combination; any such study in future will be interesting. If the computational study is extended to 3-D, for

various ramp configurations, it will be helpful to replicate the experimentally obtained pressure profiles in the reattachment zone.

REFERENCES

[1] **V. Pasquariello**, "Lehrstuhl für Aerodynamik und Strömungsmechanik Analysis and Control of Shock-Wave / Turbulent Boundary-Layer Interactions on Rigid and Flexible Walls."

[2] **S. B. Verma and M. Chidambaranathan**, "Transition control of Mach to regular reflection induced interaction using an array of micro ramp vane-type vortex generators," *Phys. Fluids*, vol. 27, no. 10, 2015.

[3] **P. Sciences and M. R. Saad**, "Experimental Studies on Shock Boundary Layer Micro-Ramps At Mach 5," 2013.

[4] **H. Babinsky and J. K. Harvey**, *SHOCK WAVE – BOUNDARY-LAYER INTERACTIONS*. .

[5] **A. Hadjadj, Y. Perrot, and S. Verma**, "Numerical study of shock/boundary layer interaction in supersonic overexpanded nozzles," *Aerosp. Sci. Technol.*, 2015.

[6] **S. B. Verma and C. Manisankar**, "Assessment of Various Low-Profile Mechanical Vortex Generators in Controlling a Shock-Induced Separation," *AIAA J.*, vol. 55, no. 7, pp. 2228–2240, 2017.

[7] **S. B. Verma and A. Hadjadj**, "Supersonic flow control," *Shock Waves*, vol. 25, no. 5, pp. 443–449, 2015.

[8] **A. A. Pasha**, "Study of Parameters Affecting Separation Bubble Size in High Speed Flows using k-ω Turbulence Model," *J. Appl. Comput. Mech.*, vol. 4, no. 2, pp. 95–104, 2018.

[9] **M. R. Saad, H. Zare-Behtash, A. Che-Idris, and K. Kontis**, "Micro-ramps for hypersonic flow control," *Micromachines*, vol. 3, no. 2, pp. 364–378, 2012.

[10] **F. K. Acquaye**, "Evaluation of Various Turbulence Models for Shock-Wave Boundary Layer Interaction Flows," 2016.

[11] **F. Lu, Q. Li, Y. Shih, A. Pierce, and C. Liu**, "Review of Micro Vortex Generators in High-Speed Flow," *49th AIAA Aerosp. Sci. Meet. Incl. New Horizons Forum Aerosp. Expo.*, no. January, pp. 1–16, 2011.

[12] **T. Herges, E. Kroeker, G. Elliott, and C. Dutton**, "Microramp Flow Control of Normal Shock/Boundary-Layer Interactions," *AIAA J.*, vol. 48, no. 11, pp. 2529–2542, 2010.

[13] **C. J. Stam**, "Source Term Modeling of Vortex Generators," no. c, p. 1, 2016.